Dipl.-Ing. Thomas Bohnstingl, BSc BSc

Physical model of low-frequency noise in Phase-Change Memory devices

MASTER'S THESIS

to achieve the university degree of

Diplom-Ingenieur

Master's degree programme: Technical Physics

submitted to

Graz University of Technology

Supervisor

Univ.-Prof. Ph.D., Peter Hadley

Institute of Solid State Physics

Graz, September 2020

AFFIDAVIT

I declare that I have authored this thesis independently, that I have not used other than the declared sources/resources, and that I have explicitly indicated all material which has been quoted either literally or by content from the sources used. The text document uploaded to TUGRAZonline is identical to the present master‘s thesis.

Date

Signature

Kurzfassung

Elektrisches Rauschen und im Speziellen das sogenannte 1/f Rauschen zählt zu den größten Störquellen und Limitierungsfaktoren für Phase Change Memory (PCM) Zellen und darauf basierende Hardwarebeschleuniger. Die Literatur weist eine Vielzahl von Forschungsgruppen auf, welche sich diesem Thema gewidmet haben, um mehr Einsicht in die beobachteten physikalischen Prozesse zu erlangen. Daraus haben sich mehrere theoretische Modelle und Beschreibungen entwickelt, welche allerdings entweder nur gewisse Aspekte des 1/f Rauschens oder die experimentell beobachteten Phänomene nicht adäquat vorhersagen. Diese Arbeit unternimmt einen Versuch, die dem Rauschen zugrundeliegenden Prozesse anhand eines in der Literatur sehr häufig verwendeten theoretischen Modells, dem Double-Well Potential, zu beschreiben. Da das elektrische Rauschen von mehrere Faktoren beeinflusst wird, wie zum Beispiel der Temperatur, der angelegten Spannung oder des Alterungszustandes der PCM Zelle, versucht diese Arbeit die einzelnen Variablen getrennt durch verschiedene Experimente zu untersuchen. Als Grundlage dafür, wurden zwei separate Plattformen zur Vermessung des Rauschens aufgebaut, wobei ein Messaufbau bei Raumtemperaturen und Temperaturen darüber hinaus operiert und der zweite bei kryogenen Temperaturen mit flüssigem Stickstoff. Durch diese beiden Messaufbauten wurde es möglich, das Verhalten des Rauschens unter verschiedensten Bedingungen zu untersuchen, mit dem Resultat, dass die Größe des Rauschens von dem Quadrat des Widerstandswertes der Probe abhängig ist. Zusätzlich wurden die experimentell beobachteten Ergebnisse mit dem theoretischen Modell verglichen, welches diese jedoch nicht angemessen beschreiben konnte. Da es bis heute in der Literatur und auch in der Forschungsgemeinschaft zum Thema 1/f noch viele offene Fragen gibt, macht diese Arbeit basierend auf den beobachteten Daten Vorschläge für weitere Experimente, um noch tiefgreifendere Einblicke erhalten zu können.

Abstract

Low-frequency noise, or 1/f noise, is one of the most limiting factors of Phase Change Memory (PCM) devices and PCM-based hardware accelerators. Several different groups have investigated this issue to gain more insights and a fundamental understanding of 1/f noise. As a result, many theoretical models have been proposed in the literature. Unfortunately, many of these models are either very specific for particular devices or fail to model the experimental data well. In this thesis an attempt is made to better understand the physical principles that underly the observed 1/f noise. After an extensive literature review, a simple yet often used theoretical model, the so-called double well potential, is be employed. Because the low-frequency noise of PCM devices is influenced by many variables, like the material composition, the temperature, the applied bias voltage and even the stage of cycling, this thesis separately investigates these variables with several experiments using different Phase-Change materials under different operating conditions and at various temperatures. To enable these experiments, two different platforms to measure the sensitive noise are built, including a setup inside a cryostat to enable measurements at cryogenic temperatures. A striking finding observed across all experiments is that the noise magnitude scales with the squared resistance of the PCM device. In addition, all the experimental data is interpreted and compared to the theoretical model. As there are still many unsolved problems in the realm of low-frequency noise in Phase-Change materials, this thesis also proposes further experiments that could be used to verify the generality of the findings and to gain more fundamental insights.

Acknowledgments

I would like to take this opportunity and thank several people without whom this thesis could not have been successfully finished. First and foremost, my supervisor Univ.-Prof. Ph.D. Peter Hadley, deserves a big honor for his dedication, unconditional availability and all the fruitful discussions with constructive feedback throughout this work. A similar gratitude is owed to my two supervisors at IBM Research Zurich, Ph.D Abu Sebastian and Ph.D Manuel Le Gallo-Bourdeau, for their guidance and valuable discussions for this work. In addition, I also want to thank my colleagues Urs Egger, Iason Giannopoulos, Benedikt Kersting and Ph.D Ghazi sarwat Syed, as well as Ass.Prof. Dipl.-Phys. Dr.rer.nat. Karin Zojer for their help and support. Finally, without the support of my family, friends and especially my girlfriend Christina Ortner, I would not have had the energy to complete this work out.

Contents

Abbreviations

AD ..... Access Device
AI ..... Artificial Intelligence
BD ..... BlueRay disc
BJT ..... Bipolar Junction Transistor
CD ..... Compact Discs
DOS ..... Density of states
DRAM ..... Dynamic Random Access Memory
DTFT ..... Discrete Time Fourier Transform
DUT ..... Device under test
DWP ..... Double-well potential
GST ..... $Ge_2Sb_2Te_5$
LE ..... Leading edge
MLC ..... Multi-level cell
MOSFET ..... Metal Oxide Field Effect Transistor
OS ..... Oscilloscope
PCM ..... Phase-Change Material
PG ..... Arbitrary waveform generator
PSD ..... Power Spectral Density
RT ..... Room Temperature
RTN ..... Random telegraph noise
SCM ..... Storage class memory
SMU ..... Source Measure Unit
TCR ..... Temperature coefficient of electrical resistivity
TE ..... Trailing edge
TLS ..... Two-Level System

1 Introduction

This master thesis deals with low-frequency noise (1/f noise) in Phase-Change Materials (PCM) and utilizes theoretical models to explain this process. To do so, the 1/f noise in mushroom cells, a type of PCM devices, is measured and compared to the Double-well potential (DWP) model. Although this model is rather simple and contains only few parameters, it has been proposed to describe low-frequency noise in other materials and was also successfully used in related problems. Moreover, the temperature behavior of the low-frequency noise will be investigated, which potentially provides new insights into the physical phenomenon.

The thesis is divided into seven chapters. The remainder of the first chapter is used for a general introduction into the topic, including applications that highlight the relevance of this work, as well as for the motivation of this thesis. The second chapter reviews the background and related literature work discussing different types of noise and the characterization method used. In addition, the PCM devices used throughout the thesis and the non-idealities thereof are discussed as well. Since this thesis focusses on low-frequency noise and the corresponding literature is rather diverse with many ongoing open discussions, a separate chapter, chapter three, is dedicated to an extensive literature review. Various approaches are discussed, their relations are analyzed and at the end a summary along with a plan how to potentially tackle some aspects is proposed. In chapter four, the theoretical model used in this thesis is introduced. It is based on the literature review from the previous chapter and allows to make predictions which could be verified experimentally. The fifth chapter deals with the experimental measurement setups necessary to conduct low-frequency noise measurements. During the course of this thesis, two separate setups have been developed. One setup for investigations under room temperature (RT) conditions and a second setup inside a cryostat to measure at temperatures well below 0°C. The subsequent chapter six aims to interpret the measured data using the theoretical model presented before and draws some conclusions. Finally, the thesis closes with a discussion in chapter seven and provides an outlook for future work regarding the investigation of low-frequency noise. This also includes additionally proposed experiments which can be conducted to gain more conclusive evidence and insights.

1.1 Applications

1.1.1 Storage devices

Over recent years, the amount of data processed by digital information systems has grown rapidly [1]. Supported by an ever-growing and faster network architecture to connect even some of the remotest places on earth, these huge amounts of data have propelled applications such as Big Data and Artificial Intelligence (AI) [2, 3, 4]. Modern applications like these have become ubiquitous in our daily life, for example when using online speech translation, voice-controlled home assistants or financial analytics and forecasting systems [5].

The data for these applications is typically stored on different types of storage devices, for example depending on the access frequency. Typically, three main types of storage devices are distinguished: Static Random Access Memory (SRAM), Dynamic Random Access Memory

(DRAM) and Flash memory.

SRAM, depicted in Figure 1.1a, has two inverters at its core. To store information in such a device, for example a logical 1, the corresponding wordline WL has to be set to a logical 1 and in addition, a logical 1 has to be applied to the bitline BL, while a logical 0 is applied to the inverted bitline $\overline{\text{BL}}$. This will force a certain configuration on the two inverters, for example the left one outputs a logical 0 and the right one a logical 1. The two inverters are coupled in such a way that the output from one becomes the input from the other and vice versa. Therfore, even if the signals are removed from the wordline WL and the bitline BL, the information is pertained in the memory cell. If the information needs to be read, the bitlines BL and $\overline{\text{BL}}$ are set to the middle value between a logical 0 and a logical 1. Depending on the stored value, one of the lines goes to a logical 1, while the other goes to a logical 0. However, if the memory cell is not constantly supplied with energy, the information is lost. Compared to SRAM, the main benefit of this storage type is the access speed, which is why it is often used for fast on-chip memory (cache) in today's computers.

DRAM, depicted in Figure 1.1b, operates by charging a capacitor to store information. For example, if a logical 1 should be stored, the capacitor is charged. If the information has to be read, the current coming from the capacitor is measured and if it exceeds a particular threshold, a logical 1 or a logical 0 is recognized respectively. No DRAM cell is flawless and leak currents reduce the amount of charge stored on the capacitor. The capacitor needs to be refreshed periodically to avoid errors, where SRAM cells are often used. Therefore, also this type of memory needs to be supplied with energy, or otherwise information is list. The main benefit of DRAM compared to SRAM is the cheaper price per bit due to the smaller area footprint, of only one transistor and a capacitor compared to six transistors. However, DRAM memory faces longer access times and is typically used as the main memory of computers.

In contrast to the two volatile memory technologies described before, Flash memory stores charges on a floating gate. Figure 1.1b shows a flash memory cell to store a single bit of information. The structure of the memory cell is similarly to a metal oxide field effect transistor (MOSFET) with two gates, a control gate and a floating gate. In the logical 0 state, no charge is present on the floating gate. If a logical 1 needs to be stored, a high voltage, on the order of several volts, is applied to the control gate and charge carriers can tunnel through the thin oxide layer onto the floating gate. If the high voltage is removed again, the charge carriers are trapped on the floating gate and cause the transistor to switch on. For example, if the memory cell is built based on a n-channel MOSFET, electrons removed from the floating gate, an inversion channel will form and switch the transistor on. Thereby, information can be stored and retrieved based on the state of the transistor. The main benefit of Flash memory is the non-volatility and the cheaper price compared to DRAM and SRAM. However, the high voltage required to write information causes device wear and limits the long term stability of the memory [6].

To further increase the storage density, one could either scale down the individual memory cells, e.g. by using newer technology nodes, or store multiple bits on the same cell, so-called multi-level cells (MLC). However, storing b bits on the same memory cell comes with the problem, that the read logic needs to distinguish between $N = 2^b$ states. Note, MLC often refers to storing only two bits on the same cell, not arbitrarily many, e.g. Triple-level cell (3 bit), Quad-level cell (4bit).

The combined variety of requirements from high storage capacity to short access times poses challenges for the storage devices, discussed above. While each technology has strengths but also limitations, there is often a tradeoff between storage capacity, reliability, and volatility to be made. To address this problem from a different perspective, researchers have investigated

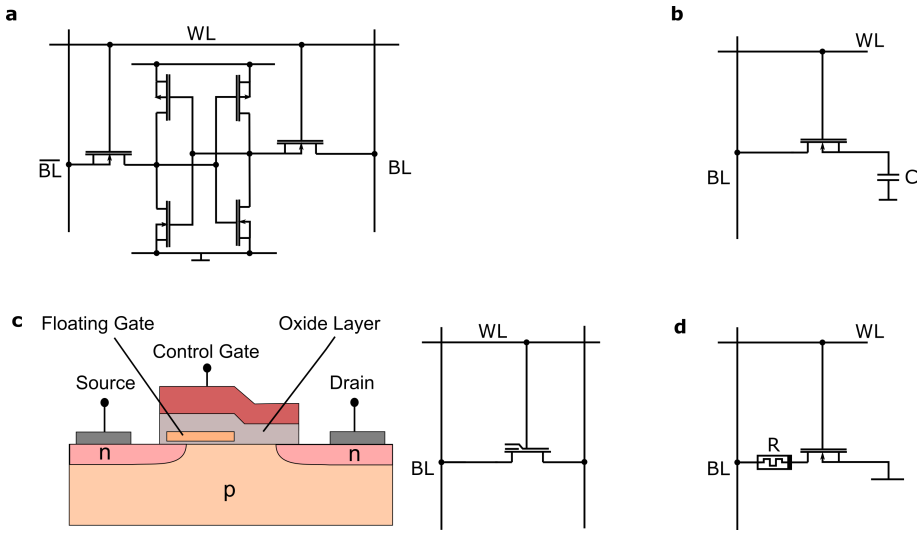

Figure 1.1: ***Schematic drawings of different memory cells.*** ***a*** *Schematic drawing of a SRAM memory cell consisting of six MOSFETs.* ***b*** *A DRAM memory block is an arrangement of memory cells that consist of an access transistor and a capacitor.* ***c*** *The flash memory cell is structured similarly to a MOSFET with two gates (a control gate and a floating gate). If a high voltage is applied to the control gate, charge carriers can tunnel through the thin oxide layer onto the floating gate and get trapped there. They can then switch on the transistor which is used to store information. Image adapted from* `https://commons.wikimedia.org/wiki/File:FLASH_RAM-Cell.svg`. ***d*** *In a PCM memory cell, the information is stored in the conductance state of the Phase-Change material. Similar to a DRAM, a single access transistor per cell is used.*

new materials to develop devices that combine the speed of DRAM with the capacity and non-volatility of Flash memory devices. One line of research has focused on so-called Phase-Change Materials. This class of materials has been known for a long time and was used commercially in Compact Discs (CDs) [7]. The essence of PCM is that it undergoes a phase transition at a certain temperature, where the phase configuration changes from an amorphous state to a polycrystalline state and the other way around. These phases yield different conductance values which are used store information, for example a low-conductance state indicates a logical 0, while a high-conductance state indicates a logical 1. If the PCM is in a polycrystalline phase and gets heated enough, it starts to melt and transits to a liquid phase. When cooled quickly to room temperature, it freezes into an amorphous glass state (amorphous phase). As already mentioned, the polycrystalline and the amorphous phase exhibit different electrical and optical properties. For example, a CD is made of PCM. To store information, the material is transformed into an amorphous state in particular locations with an intense laser. Later, a weaker laser is used to detect differences in optical reflections and thereby reads the stored information on the disc. PCM devices can also be used for MLCs and store more than a single bit of information by using multiple conductance states [8] (see Section 2.2 for more details).

Today, an entire class of memories is being formed around so-called storage class memory (SCM) [9]. Not only PCM-based storage devices fall into this category, but also other emerging non-volatile memory technologies, such as resistive RAM (ReRAM) [10] or magnetic RAM (MRAM) [11, 12, 13]. These devices have in common that firstly, they are non-volatile memory elements, secondly, the provide access times slower than traditional DRAM, but much faster than SSDs or HDDs and lastly, that they are cheaper than DRAM or SRAM.

1.1.2 In-memory computing

In addition to pure utilizing memory for pure storage applications, modern applications challenge the traditional computing architectures based on the von Neumann architecture in general. In von Neumann architectures, the memory, which stores the information, is separated from the central processing unit (CPU) that executes instructions based on data fetched from the memory. With ever increasing amounts of data to be processed, the effort of moving data between the CPU and the memory becomes a limiting factor [14]. Note that although the CPU itself hosts memory on-chip, in fact almost half of the area of a modern CPU is dedicated to SRAM memory, so-called cache memory, but it is limited to a few hundred kB in size. In modern applications, the amount of data processed is on the order of GB or larger and therefore needs to be stored in an external memory [15].

One avenue to address this problem is in-memory computing where memory and computation are collocated into a single element, so-called computational memory [16]. This represents a fundamentally different way how computation is performed. Unlike in the von Neumann architecture, the data is not moved between the memory and the CPU, but instead the instructions to be executed on the data is moved from the CPU to the computational memory. The memory then performs this operation with the data in place [17].

One possible realization of an in-memory computing architecture is using the aforementioned PCM devices [14, 18]. For example, if these devices are arranged in a crossbar architecture, certain operations can be performed with the data in place (see Section 2.2 for more details).

1.2 Motivation

PCM is a memory technology in an advanced state of research with several potential target applications, like the two which have been outlined above. Memories of this kind target the gap between DRAM and Flash memory and have already been demonstrated in several applications. However, storing multiple bits on the same PCM device and using them as a computational memory element, imposes requirements for the reproducibility, long-term stability, and precision. Fabrication problems, for example device-to-device variabilities, and other imperfections pose challenges that need to be solved. In addition to these issues which also appear often in other electronic devices, PCM devices face two more fundamental problems that emerge directly from the physical properties and pose the main limiting factors.

One of these problems is that the conductance state of the device drifts over time. This problem becomes especially apparent when storing multiple bits on a single device. For example, if the PCM device is used as an MLC, four distinct conductance levels must be separable. If the conductance state drifts enough over time so that it reaches from one state into another, the information is effectively lost. This phenomenon has been studied in recent years and a good understanding has been developed, see Section 2.2.7 for a further discussion.

The second problem is low-frequency noise, often also called 1/f noise, that is observed in PCM devices, see 2.2.7. Like any other type of noise, it impairs the precision with which information can be retrieved from the device. However, the special property of 1/f noise is that its magnitude depends inversely on the access frequency of the individual cells. Therefore, the 1/f noise essentially limits applicability of PCM-based storage devices. For example, in applications where PCM devices are used for in-memory computing, the 1/f noise is the limiting factor for the precision of the matrix-vector operations.
Although the 1/f noise has an impact on the overall performance of PCM devices, like the drift phenomenon, its understanding is much more limited. A profound theory is either lacking or fails to explain experimentally observed data well under various conditions. Therefore, the present

master thesis has set its goal to study the observed 1/f-noise and to investigate theoretical models that could explain this data. Such a model would potentially:

- Result in a better understanding of the behavior of the 1/f noise under different operating conditions, for example elevated temperatures.
- Devise mechanisms to compensate for the noise, for example through external electrical circuitry.
- Have a high value for the community and
- Enhance the overall usability of PCM devices, for example in applications like in-memory computing.

Throughout this thesis, the low-frequency noise is investigated from various angles in several experiments with the common target to gain more insights into the underlying physical principles.

2
Background

This chapter is split into two parts. First, electrical noise, its properties, important types of noise and ways how to measure them are explained and discussed. After this basis has been established, the second part focusses on Phase-Change Materials. This part outlines in a detailed manner what a PCM is, what the key characteristics are, what underlying physical mechanisms play important roles and what the non-idealities and shortcomings are. After this chapter, the foundation for the remainder of the thesis should have been laid.

2.1 Electrical noise

Fluctuations of electrical signals, such as fluctuations of voltage or current amplitudes, are called noise and are a fundamental property almost any electronic device exhibits [19]. For example thermal noise, so-called Johnson noise [20, 21], is experimentally observed in wide variety of materials and was described by a theory shortly after its discovery. There exist also other types of noise such as Shot noise [22], Burst noise or Flicker noise (1/f noise or low-frequency noise) [23, 24] which may have different physical origins and will be discussed in the following. Often in practice, the observed noise is a superposition of different types of noise. For example if a bias voltage is applied on a resistor, the resulting noise will consist of the thermal noise of the resistor and in addition, the voltage source might exhibit high frequency noise spikes due to its power supply which are also visible in the noise of the resistor.

2.1.1 Noise characterization

One method to characterize, compare and distinguish different types of noise is to compute the power spectral density (PSD) [25]. The PSD can be calculated using the Fourier Transform on the signal and is a measure of how much power is present at different frequency components. This subsection aims to introduce the notation of the PSD, as this is the key quantity used in later chapters of this thesis, see [26] for more in-depth details. To begin, the noise signal $\{y(t); t = 0, \pm1, \pm2, ...\}$ is assumed to be a discrete time random sequence, in the sense that the variation over time cannot be predicted. Therefore, only probabilistic statements can be made. Because of this assumption the noise signal, which represents a single realization of a random sequence, does not have finite energy, i.e. $\sum_{t=-\infty}^{\infty} |y(t)|^2 = \infty$ and thus a discrete Fourier transform (DTFT) does not exist. However, the average over multiple realization of this signal has finite power and a DTFT for this average signal exists. When speaking of the PSD of a noise signal, one refers to the average PSD. Furthermore, another important quantity is the autocorrelation function (ACF) of the signal, given as

$$r(\tau) = E\left\{y(t)y^*(t+\tau)\right\}. \tag{2.1}$$

With this definition, the Wiener-Khintchine theorem [27, 28] can be used and the PSD of a stationary random process of finite length N can be defined as

$$S(\omega) = lim_{N\to\infty} E\left\{\frac{1}{N}\left|\sum_{t=1}^{N} y(t)e^{-\imath\omega t}\right|^2\right\}, \tag{2.2}$$

where $E\{\cdot\}$ denotes the expectation value and ω denotes the angular frequency. As mentioned before, this can be seen as the DTFT of the ACF of the noise signal $y(t)$. This can also be expressed in terms of the frequency f instead of the angular frequency ω

$$S(f) = lim_{N\to\infty} E\left\{\frac{1}{N}\left|\sum_{t=1}^{N} y(t)e^{-\imath 2\pi f t}\right|^2\right\}. \tag{2.3}$$

In practice, depending on the setup and the device, different fluctuations are measured, i.e. the voltage fluctuation, the current fluctuation, the resistance fluctuation or the conductance fluctuation. For example if the voltage fluctuation is measured, $y(t) = u(t)$, the power spectral density $S(f)$ is then denoted as $S_U(f)$, S_U for short, and its unit is $\frac{V^2}{\text{Hz}}$. Note that a similar notation is used for the PSD of the other fluctuations. However, often in experiments the normalized PSD $\frac{S_U}{U^2}$ with the unit $\frac{1}{\text{Hz}}$ is reported, to facilitate better comparability. Note that the normalized noise spectra can be equivalently obtained through the following relations

$$\frac{S_U}{U^2} = \frac{S_I}{I^2} = \frac{S_R}{R^2} = \frac{S_G}{G^2}. \tag{2.4}$$

Figure 2.1a shows a example time signal and Figure 2.1b shows the corresponding PSD. The

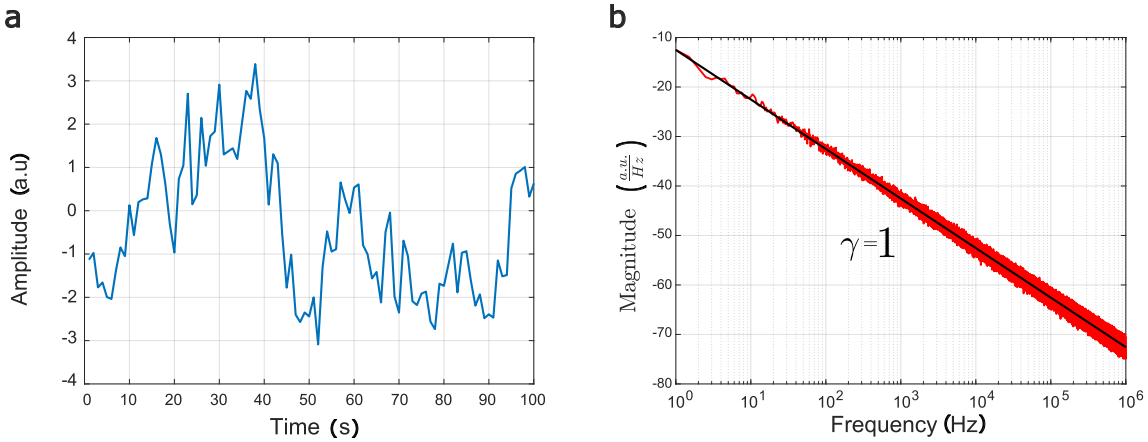

Figure 2.1: ***Time sequence and corresponding Power Spectral Density of 1/f noise.a****, First 100*s *of a time signal.* ***b****, Corresponding PSD of the time signal from* ***a*** *with a fit of the slope.*

noise shown in these two plots is of a especially relevant for this thesis (1/f noise), which will be discussed in Section 2.1.2 and in Chapter 3 to a great extent.

2.1.2 Types of noise

The Power Spectral Density as explained above can be used as the characterization method to distinguish different types of noise signals that would not be possible in the time domain. For example, Figure 2.1a and Figure 2.2a show two different times signals which can hardly be distinguished. However, their respective PSDs in Figure 2.1b and Figure 2.2b clearly differs.

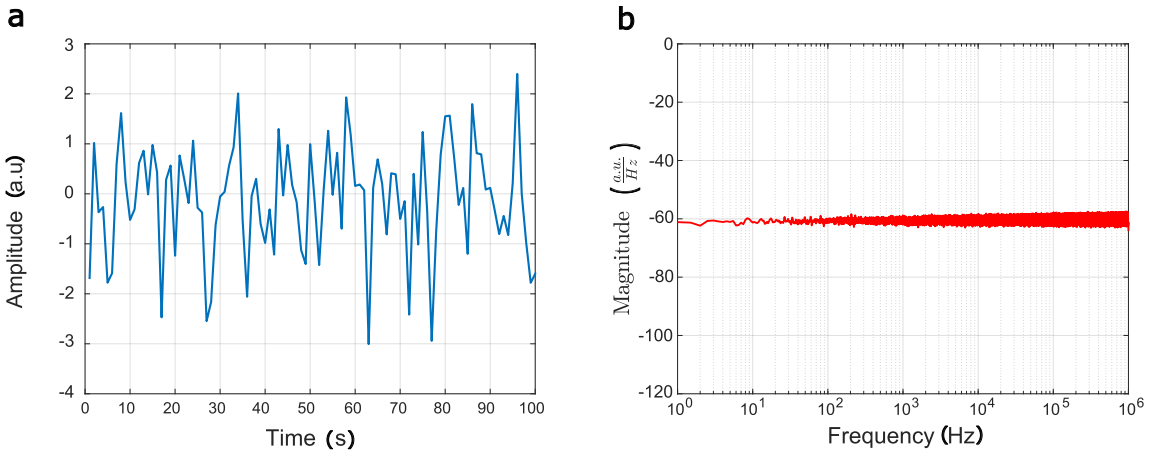

Figure 2.2: ***Time sequence and corresponding Power Spectral Density of white noise.a****, First 100* s *of a time signal.* ***b****, Corresponding PSD of the time signal from* ***a****.*

These two figures demonstrate two important types of noise that can be found in various electronic devices. Arguably the simplest type of noise is the thermal noise, or Johnson noise, which is exhibited by electrical resistors [20, 21]. Moreover, this type of noise is present in all electrical circuits and is sometimes the limiting factor for sensitivity, for example in amplifiers or radio signal receivers. Its PSD can be computed as a function of the temperature T and the resistance value R as

$$S(T, R, f) = 4k_b T R, \tag{2.5}$$

where k_b represents the Boltzmann constant, T is the temperature and R is the resistance value. Therefore, an electrical resistor shows a constant PSD, see Figure 2.2b, across a wide range of frequencies. Another important fact to mention is that the thermal noise is independent of the applied voltage and only depends on the resistance value. However, there are physical limits, for example for very high electrical fields the resistor may break down. The simplified picture of the physical origin for this type of noise is that at temperature above absolute zero, the charge carriers in a conductor exhibit random vibrations which translates to a fluctuating potential at the ends of the conductor and therefore the random fluctuations are present irrespective of the applied voltage. If an electrical field is applied, the charge carriers do not flow in a straight line through the conductor, but the motion is disturbed by the random movements, which manifests itself in a fluctuation of the current.

1/f noise

The second type of noise depicted in Figures 2.1a,b is the so-called low-frequency noise, 1/f noise or flicker noise [29]. This type of noise features a PSD with particularly pronounced contributions at low frequencies, hence the name. It can be described as

$$S(f) = Q f^{-\gamma}, \tag{2.6}$$

where Q is a constant and γ is the slope exponent. Note that both, the constant Q, as well as the slope parameter γ may depend on the material and the measurement setup, for example the temperature T. This type of noise was observed in vacuum tubes [29], in semiconductors [30] and even in non-electronic devices, such as in biological systems [31] or in stock markets [32]. Despite the ubiquitous nature of this type of noise, we will restrict the investigations to the domain of electrical devices in the following.

Due to the particular frequency dependence, 1/f noise is typically only prominent at lower frequency and overshadowed at higher frequencies by other noise mechanisms, such as the thermal noise. In this superposition, a corner frequency f_c can be assigned to the 1/f noise which is the point that separates the dominant low-frequency components from the flat thermal noise, schematically illustrated in Figures 2.3a,b. Since the topic of 1/f noise is of general interest, not

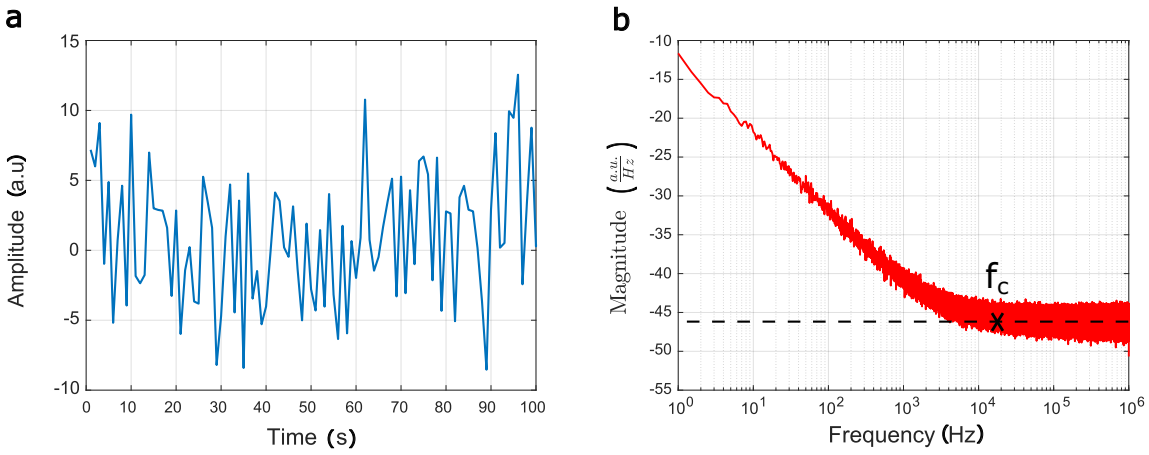

Figure 2.3: ***Time sequence and corresponding Power Spectral Density of white noise superimposed by 1/f noise.a****, First 100*s *of a time signal.* ***b****, Corresponding PSD of the time signal from* ***a****.*

only for PCM devices, the entire Chapter 3 is devoted to explaining the detailed specifics of the theories and models from literature.

Random telegraph noise

Random telegraph noise (RTN) is another type of noise that shows a very peculiar time signal illustrated in Figure 2.4. The current signal appears to jump between two discrete levels at

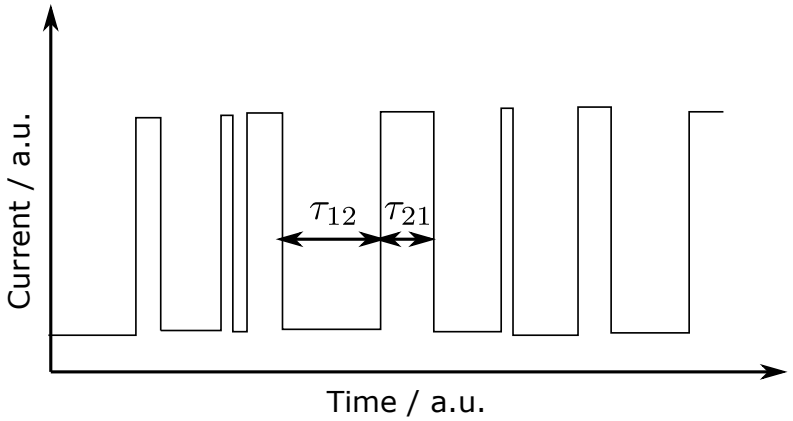

Figure 2.4: ***Example current signal for random telegraph noise.*** *The characteristic transition times from the lower to the higher level and vice versa are indicated with* τ_{12} *and* τ_{21} *respectively.*

random time intervals without reaching any stable state. This process can be observed in various electrical devices, such as MOSFETs and also PCM devices [33, 34, 35]. The physical origin of this noise is believed to be the trapping and detrapping process of individual charge carriers. However, the detailed nature of the trapping and detrapping process is still subject to investigations [34]. In PCM devices the RTN is most present in the intermediate states, where

the material is neither in a fully polycrystalline nor a fully amorphous state, see Section 2.2. As we will see in Chapter 3, the two characteristic transition times from the lower level to the higher level τ_{12} and vice versa τ_{21} were modelled in theory.

2.2 Phase-Change Material

Phase-Change materials are a novel class of materials that show different behaviors compared to traditional semiconductors. Since PCMs are at the very heart of the present thesis, this section is intended to discuss the details of these materials.

2.2.1 Material composition

PCM are typically chalcogenide alloys, mostly consisting of three elements Ge, Sb and Te, which can be represented in a ternary phase diagram [36]. First alloys, that are still used today, were already proposed in the 60s [37]. A few examples are Sb_2Te, $Ge_2Sb_2Te_5$ (GST) and $Ge_8Sb_2Te_{11}$ [7, 36, 38]. In this thesis GST will be used and therefore the following discussions on the crystal structure and the electrical transport mechanism will be based on this material. One advantage of this material is that it is quite well-studied in the literature in terms of the crystal structure, the temperature behavior as well as the electronic band structure.

The properties of the PCM, such as the lattice constant, optical properties or the melting temperature critically depend on the composition. For example, as briefly mentioned in the introduction, Phase-Change Materials were initially developed for storage devices, such as DVDs. In this case GST is used as the PCM, but for BlueRay discs (BD) lasers of shorter wavelengths, for example the blue-violettish 405nm, are used to increase the storage density [39]. This also influenced the choice of the PCM and in the case of BD $Ge_8Sb_2Te_{11}$ is used [36].

However, there are many more target applications for PCM devices besides DVDs and BD, for example the applications of in-memory computing or storage-class memory mentioned in Chapter 1.2. In these various applications it is not clear which compound is ideal and yields the best properties. One general observation in GST-based PCM devices has been that this material requires high reset currents, faces a thermal stability issues and provides only limited retention rates.

Therefore, researchers are exploring different material compositions and also experiment with doping to improve certain properties [40, 41, 42, 43, 44, 45, 46, 47]. Doping is a commonly used technique to improve electrical properties of traditional semiconductors, where doping increases for example the conductivity of an undoped semiconductor which is essential for building devices such as MOSFETs. Similarly, doping is a very common technique to change the electrical properties of PCM devices. Especially, it improves the efficiency of the phase switching between the crystalline and the amorphous one. For example, when using carbon doped GST as the PCM, the data retention and switching currents can be reduced. Another example is that SiO_2 doped GST devices, require less power to amorphize the material, e.g. by using a lower pulse amplitude while using the same temporal pulse shape. This property originates from the melting temperature being significantly lower for the doped GST compared to the undoped GST. In addition, it was also observed that the crystallization temperature of the PCM device increases. This originates from an increased activation energy for the crystallization process because doping suppresses the crystallization effect [44]. Recently, transition metals used as dopants have demonstrated the potential to greatly improve the performance of PCM devices. Especially increasing the efficiency is desired for building large scale chips based on PCM devices, as less power is dissipated, and the overall energy-efficiency of the system is increased.

However, doping also introduces additional defects. For example, doping in GST devices often comes with a higher risk of phase segregation, which could cause undesired behaviors and malfunctions of the devices [46]. In addition, doping creates also more trap states in the material. These additional defects also increase the noise of the PCM device, which will be

experimentally investigated in Section 6.3. This increased noise level has a negative impact on the performance of a PCM-based chip, because, like mentioned in the introduction, the noise of the individual devices essentially limits the overall precision level of the chip.

In addition, the explained effects of doping depend on the doping concentration as well as on the deposition method [42]. For example, it has been observed that as the doping level is increased, the melting temperature is also successively reduced [44].

The experimental part of this thesis mainly investigates GST as the PCM for the devices, but also with various doping concentrations. To properly annotate the material used in an experiment, we will use the term 'GST' for pure GST and 'dGSTxxx' for doped GST, where 'xxx' are three digits referring to the doping level. In this notation, higher numbers indicate a higher doping level. For example, 'dGST300' and 'dGST400' both indicate doped GST , but the latter one is more heavily doped.

2.2.2 Phase switching

The process responsible for the phase change can be described with multiple steps and is outlined in the following. Consider the device to be initially in a polycrystalline state at RT. This means that the atoms of the PCM are arranged similar to a crystalline structure with a long-range order, but grain boundaries may exist, and a perfect crystal might not form. However, due to this long-range order, charge carriers can flow relatively easy through the material and the conductivity in this state is high [36]. If a current is supplied through the AD to the HE, the temperature in the PCM increases due to resistive heating (Joule heating). Above the melting temperature T_m of the PCM, typically around 600°C for GST, a phase transition from the solid phase to the liquid phase occurs. In the liquid phase, the polycrystalline structure is lost, and an unordered structure emerges. If the PCM is cooled rather quickly to RT again, the mold is 'frozen' and the atoms are stuck in an amorphous, glass-like, state rather than arranging themselves into a polycrystalline structure. This process is called melt-quenching and is a well-known technique to create amorphous glasses [36]. The electrical pulse used to achieve this melt-quenching is called a RESET pulse, as it causes the PCM to transition from a SET state, polycrystalline state, to an amorphous RESET state.
Since the amorphous state does not exhibit a long-range ordering, the charge carriers exhibit a higher resistance when traversing through the material and a lower conductance, compared to the polycrystalline state, results. The different electrical properties of these two states are exploited to store information. Note that as already mentioned in the introduction, also other physical properties such as optical properties change during the phase transition, for example the optical properties are used in CDs.

If the temperature in the PCM is raised to a lower temperature T_c, between 100°C and 150°C for GST, using an electrical pulse of lower power (called a SET pulse), the amorphous material starts to crystallize again. This means that the atoms arrange themselves and the material gradually goes back to the polycrystalline phase again. Figure 2.5a illustrates the pulses and their shapes that are applied to change between the different phases. Figure 2.5b shows a so-called programming curve of a PCM device. This graph illustrates the evolution of the device conductance as a function of the applied pulse, where the temporal pulse shape is fixed, but the pulse amplitude is gradually increased. The device starts in the poly-crystalline SET state and undergoes a phase transition towards the amorphous RESET state, if the applied pulse increases the temperature of the material enough.

Table 2.1 lists properties of the SET and the RESET pulses that are typically used. One can see that while the leading edge (LE) is similar for both pulse types, their trailing edge (TE) is significantly different and is mainly responsible for the melt-quench effect. As explained above, a short trailing edge leads to a rapid cooling of the material, effectively freezing the present atomic arrangement in place, which will lead to the RESET state. In the contrary, if a long

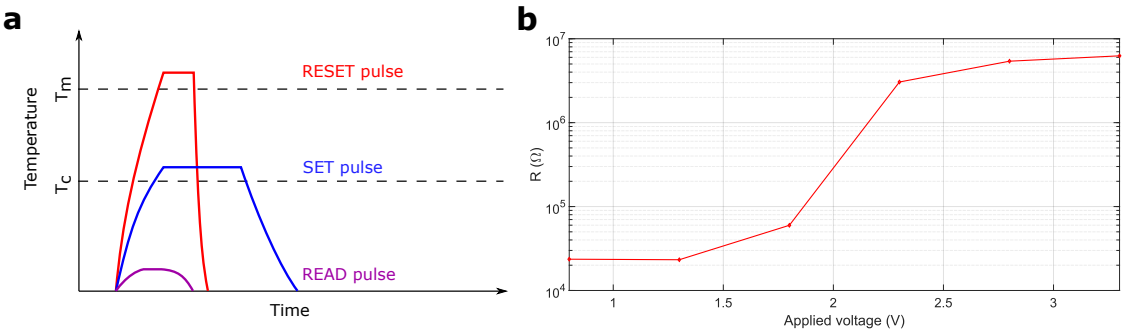

Figure 2.5: ***Effect of electrical pulses applied to PCM devices.*** *a If the PCM is heated above the melting temperature T_m and then quickly cooled back to room temperature, an amorphous phase is created. If the PCM is subsequently heated above the crystallization temperature T_c, the material crystallizes and gradually transforms back to the polycrystalline phase.* ***b*** *Programming curve of a PCM device where RESET pulses with varying voltage amplitudes are applied to an initial SET state.*

trailing edge is used and the temperature caused by the pulse is not too high, a crystallization process is creating a poly-crystalline SET state. Note that the exact electrical properties of the two pulse types depend on the size of the PCM cell, its volume, the material composition and other device specific parameters. Furthermore, it has been reported in literature that the

Table 2.1: Properties of the electrical pulses

Type	Duration / ns	Amplitude / V	LE / ns	TE / ns
RESET	100	3	10	10
SET	100	2.5	10	500

duration of these pulses can be significantly reduced to $40 - 100$ ns for a SET pulse and 700 ps for the RESET pulse, respectively [48].

As described above, the PCM can change the phases from a polycrystalline to an amorphous and back again, when proper pulses are applied. However, these phase transitions are not symmetric in both directions. While the transition from the amorphous phase to the polycrystalline phase happens gradually, the transition from the polycrystalline to the amorphous phase happens abruptly, because of the melt-quench process. However, both processes happened relatively fast, on the order of a several hundred nanoseconds. Figure 2.6 illustrates the ongoing processes when subsequent SET pulses are applied to the PCM, followed by a RESET pulse. The phase

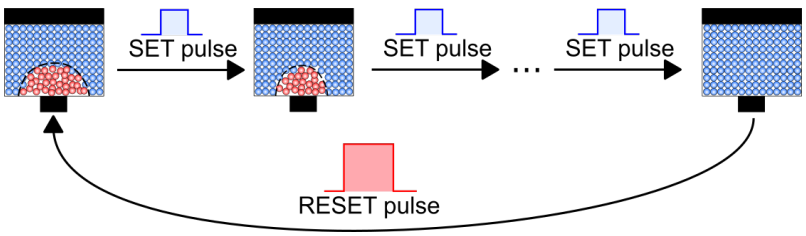

Figure 2.6: ***Effect of set and reset pulses on the PCM.*** *Subsequent set pulses initiate a crystallization of the PCM which reduces the amount of the amorphous phase. A reset pulse induces a melt-quenching and creates a region of the amorphous phase again.*

configurations between the fully polycrystalline SET state and the amorphous RESET state are often referred to as intermediate states. In this regime, the atoms of the PCM are neither

arranged in a crystal lattice, nor are the fully disordered. In contrast, there are parts of the material that are in the polycrystalline phase and there are parts that are in the amorphous phase. As we will discuss in Section 2.2.5, the polycrystalline parts will form on top of one electrode of a mushroom cell or in the center of a line cell [49]. The polycrystalline region will begin to form where the temperature is the highest and exceeds the crystallization temperature T_c.

When reading the conductance state of the cell, a read voltage, often also referred to as bias voltage, is applied which is used in combination with the resulting current to deduce the conductance state of the PCM cell.

However, one has to ensure that the current phase configuration of the PCM is not accidentally distorted through this procedure. This is especially important if the device is not in a fully polycrystalline state. If a voltage is applied across a device in a partly amorphous device, a current flows which causes Joule heating and an increase in the local temperature. If the voltage is increased a positive feedback loop arises and the material eventually undergoes the phase transition from the amorphous to the polycrystalline state. This effect called threshold switching, causes a rapid increase in the current flow, because the material changes its phase from the amorphous to the polycrystalline phase which can be observed experimentally[50, 51]. Therefore, when reading the cells conductance state, the applied voltage should be low enough to not cause the temperature of the PCM to rise above T_c or T_m, in order to avoid crystallization or melting effects. This low voltage which is applied for only a short period of time, results in a low power pulse applied to the PCM compared to the RESET and the SET pulses.

2.2.3 Crystal structure

The crystal structure of GST has been studied only many years after it was discovered [42, 52]. Yamada et. al. in their publication pointed out that GST arranges in the same crystal structure as NaCl, where one fcc-sublattice, the 4(a) site, is solely occupied by Te atoms and the second fcc-sublattice, the 4(b) site, is randomly occupied by Sb and Ge atoms. Figure 2.7 illustrates the crystal structure of GST. However, the precise stoichiometry of GST theoretically results in vacancies when forming the rock-salt crystal structure. This was also confirmed by the studies of Yamada et. al., where they analyzed variants of GST, namely $Ge_2Sb_{2+x}Te_5$ with $x = \{0.0, 0.3, 0.5, 1.0\}$. They concluded that there are indeed vacancies of around 20% present in the Sb/Ge sublattice. Moreover, the observed that even if these vacancies are present, the excess Sb atoms did not enter the NaCl crystal structure to fill the vacancies, but they remained at the grain boundaries.

In a review work, conducted by Guo et. al. [42], the question how the switching behavior affects the crystal structure of the material was investigated. It was found that the material switches between three different crystal structures. For this study the PCM was annealed at different temperatures to mimic the effects of the current pulses in a more controlled way. Initially the material is in the amorphous glass state, without any long-range order. As outlined already, the conductivity in this state is rather low, because charge carriers cannot easily pass through the material. If the temperature reaches the crystallization temperature of the material, the atoms start to arrange into the fcc structure as illustrated in Figure 2.7. This transition of the crystal structure is also accompanied with a steep increase in the conductivity, as a long-range order starts to emerge. The PCM continues to be in this phase until around 250°C and 300°C, where another structural transition to the high-temperature hcp crystal structure occurs.

The phenomenon that GST has to crystalline phases is also studied in other works [53]. It was found that this transition happens gradually because the fcc structure is only metastable, whereas the hcp structure is stable for high temperatures. Their analysis shows that a small fraction of the hcp phase is present even at lower temperatures, but outweigh by the fcc phase. As the temperature is increased, an increasingly large fraction of the PCM takes the hcp structure

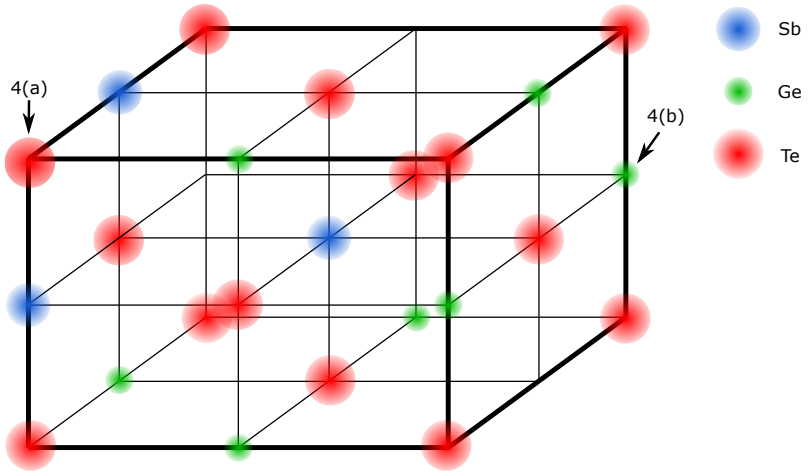

Figure 2.7: ***Example crystal structure of GST.*** *$Ge_2Sb_2Te_5$ takes on a meta-stable rock-salt crystal structure where Te atoms occupy the 4(a) sublattice and Sb and Ge randomly occupy the 4(b) sublattice.*

rather than the fcc structure. Figure 2.8

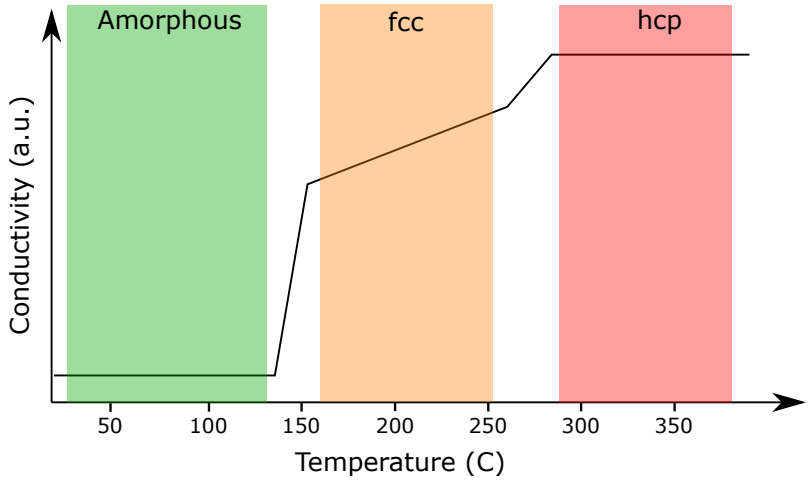

Figure 2.8: ***Change of crystal structure as a function of temperature.*** *Results schematically illustrated from [42].*

2.2.4 Band structure

The electronic band structure of GST has also been investigated in the literature [54]. One interesting feature observed in PCM materials is that even in the poly-crystalline phase, the valence and conduction band behave differently from common semiconductors, where in the latter case, the bands follow a square root dependency for 3D materials close to the band edges. PCM devices do not have a perfect crystal structure and local differences in bond lengths or angles impact the bands and cause the band edges to be less clear defined. In fact, models of the density of states (DOS) consider extended band edges that reach into the band gap due to the local defects [54]. It has been argued in literature whether the transition of the DOS arising from localized and delocalized states occurs continuously [55, 56]. In this model, one can think of a smooth transition from the square root behavior of the DOS for the delocalized states to an exponentially decreasing DOS arising from the localized states as illustrated in Figure 2.9.

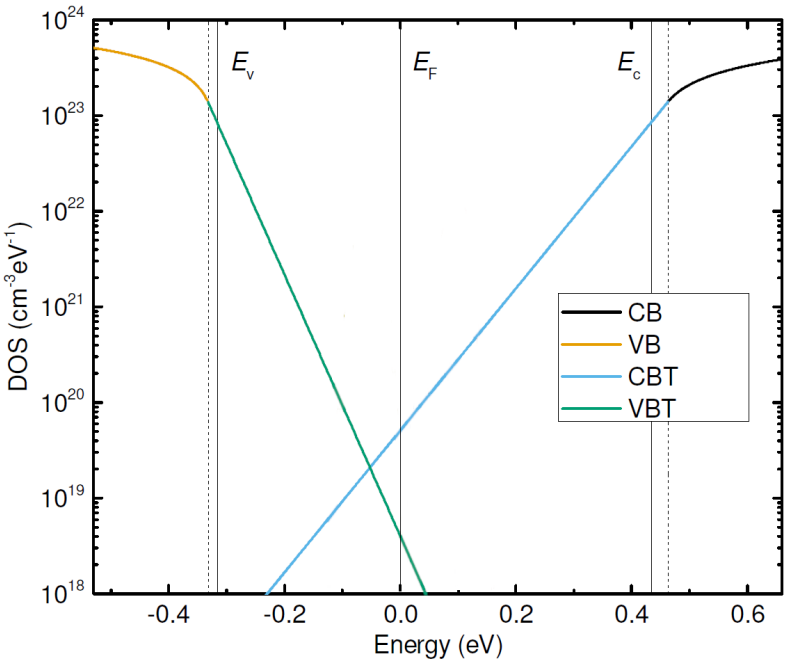

Figure 2.9: ***Illustration of density of states in a PCM.*** *The common square root behavior emerging from delocalized states is extended with an exponentially decreasing density of states due to the localized defect states. This figure is adopted from [56].*

2.2.5 Device structures

PCM devices are mainly fabricated in two structures, a mushroom cell and a line cell [57], schematically illustrated in Figure 2.10a and Figure 2.10b respectively. Figure 2.10c illustrates an arrangement of the PCM devices that can be used as a storage device.

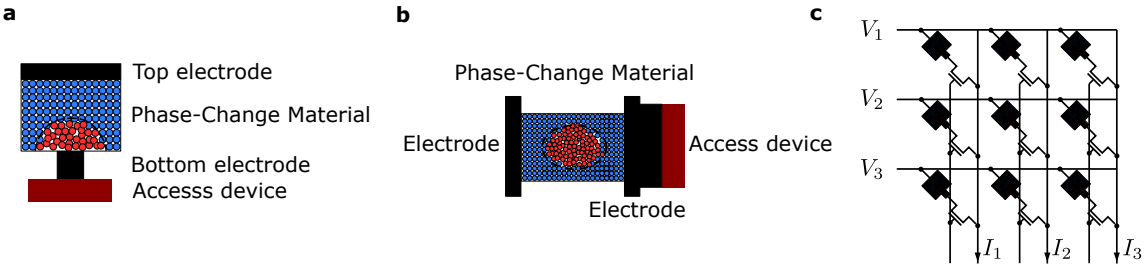

Figure 2.10: ***Different PCM device structures and example arrangement for storage.a****, Mushroom PCM cell. The PCM is placed between the top and the bottom electrode, which also functions as the heater. The access device below the bottom electrode, typically a transistor, is used to control the access to the PCM device.* ***b****, Line PCM cell. The components involved are similar to the mushroom cell, but the line cell has a planar structure.* ***c****, Crossbar arrangement of PCM devices, where a voltage is applied on the rows and a current is flowing along the columns, depending on which PCM cell is selected. This architecture can be utilized to perform in-memory operations.*

Note that the present thesis will deal with mushroom cells and hence the results will focus only on these devices. However, the basic physical principles are similar for both devices.
The main difference between these two structures is the geometry and where the PCM is placed. In both cases, the main components are the Phase-Change Material, two electrodes and an access device (AD). The PCM is placed between a top electrode (TE) and the bottom electrode (BE) which acts as the thermal heater (HE). The heater is usually smaller than the PCM and is

used to heat the material to its melting or crystallization temperature. If multiple PCM cells are connected to form a memory, it is crucial to be able to address each cell individually. Therefore, the BE is connected to an access device (AD) which is typically a MOSFET, a Bipolar Junction Transistor (BJT), or a FinFET. The AD has essentially two tasks, firstly it enables individual addressing of individual cells, as it is connected to word and bitlines and secondly it regulates the current that is supplied to heat the PCM. Moreover, the AD is a critical component for designing storage devices using PCM cells. This is because the current regulation greatly influences the size of the transistor and in consequence the density of the storage device. A large AD will decrease the storage density, as the AD will dominate the size of the storage cell and one can put fewer devices on the same area. The supplied current should be high in order to melt the PCM quickly, but as small as possible to keep the area footprint low. Therefore, one has to make a tradeoff between the current that can be supplied to the PCM and the size for the AD.

2.2.6 Transport mechanism and electrical conduction in PCM materials

The electric transport mechanism in PCM devices is different from metals, where band transport dominates and the electrons and holes in the conduction and valence band can move long distances with a certain mobility μ_e and μ_h, respectively. In PCM devices trap-limited band transport is observed which emerges due to the localized defect states [58, 59]. In this picture the charge carriers cannot move infinitely large distances in the conduction and valence band due to trapping and detrapping processes. Thus, the localized states act as limitations of the band transport. Furthermore, in the amorphous state the conduction is solely based on the local trap state [60]. Therefore, the trap states play an important role for the electrical properties of the PCM.

In addition, the position of the Fermi energy is determined to a large degree by the localized states and if it is found to be in the delocalized states then the material behaves like a metal, while if it is located in the localized states, the material behave like an insulator. Since the distribution of the localized states may change with temperature, the position of the Fermi energy is also strongly temperature dependent and consequently also the electric transport behavior of the PCM.

Different electrical transport mechanisms have also been investigated by Kaiser in [61]. Figure 6 of this work compares the behavior of the resistance of materials as a function of temperature. This figure highlights the so-called Mooji correlation which empirically states that the sign of the temperature coefficient of electrical resistivity (TCR) depends on the magnitude of the resistivity of the material [62]. Although this correlation was found to be present in various material ranging from glassy to liquid materials, the magnitude of the resistivity threshold can differ between $50 - 400\mu\Omega$cm [63, 64]. A typical value of resistivity threshold which is often used is $150\mu\Omega$cm. Above this threshold the resistance of a material increases as a function of temperature and below it decreases.

The bias voltage applied to the cell also plays an important role. First, as previously indicated in Section 2.2.2, if the voltage exceeds the threshold voltage of the device, the state is altered and the PCM cell switches to a low-resistive SET state. Therefore, if the device was programmed to a particular state and this state should be read out at a later time, the bias voltage must not exceed the threshold voltage. Secondly, PCM devices obey an ohmic as well as an non-ohmic region. The latter one is characterized by a nonlinear response to an applied voltage of the device [65]. If the current serves as the indicator of the device state, it has to be ensured that the device is read in the ohmic region, as otherwise the state is wrongly estimated. Thirdly, similarly to the material composition, the bias voltage influences the energy-efficiency of the device, respectively of the overall system. For example, if only the current state of the PCM device should be read in the ohmic region, then a higher bias voltage would yield the same information, but would dissipate more power over the device, degrading the energy-efficiency. Finally, the bias voltage

influences also the current generation mechanism of the PCM and thereby also influences the observed noise [59, 60]. The impact of the bias voltage on the low-frequency noise will also be investigated experimentally in Chapter 6.

2.2.7 Non-idealities in PCM materials

Electronic devices face fabrication variabilities, such as low fabrication yield or in device-to-device variabilities, stemming from fabrication processes that are not fully under control. However, PCM devices store information in their phase configuration, i.e. in their conductance state, which is fundamentally different from other storage devices. As mentioned already, they provide certain benefits, for example in terms of non-volatility, but in addition to the other fabrication variabilities, they bring along two fundamental problems that arise directly from the physical properties of the devices. This section first discusses the conductance drift phenomenon observed in PCM devices in Section 2.2.7 and later Section 2.2.7 discusses the electrical noise observed in PCM devices.

Conductance drift

It can be observed that the conductance value of intermediate states, i.e. states that are neither fully amorphous nor fully polycrystalline, is not stable over time. A relaxation process happens over time which causes a gradual change in the conductivity of the device [66]. This phenomenon has a direct impact on the information stored, because PCM devices often store more than one bit and the conductance drift might cause the separation between the individual levels to blur out. The deficiency becomes more pronounced the more bits are stored on the device, as the spacing between the conductance levels decreases exponentially. For example in a theoretical PCM device with a minimum conductance of 0μS and a maximum conductance of 20μS, the separation between two levels storing two bits is $\Delta S = \frac{20\mu\text{S}}{2^2} = 5\mu\text{S}$ and storing three bits is $\Delta S = \frac{20\mu\text{S}}{2^3} = 2.5\mu\text{S}$. Several variables influence the relaxation of the material, such as the conductance state itself, the time and also the ambient temperature. At a constant ambient temperature, the drift can be empirically described using the varying resistance

$$R(t) = R(t_0)\left(\frac{t}{t_0}\right)^{\nu_R}, \tag{2.7}$$

where t is the time the state of the PCM is observed, t_0 is the time at which the state of the cell was modified, $R(t)$ and $R(t_0)$ are the resistance values of the cell at time t and t_0 respectively and ν_R is the drift exponent. The drift exponent is typically a small quantity in the range between $0.01 - 0.10$ [67]. The observation is that conductance drift occurs mainly in the amorphous state, in particular, the larger the amorphous material and the lower the conductance value, the more pronounced the drift effect is [59]. To address this problem, recently a novel type of so-called projected PCM devices has been studied [68]. In these devices, a layer of a non-insulating material, a so-called projection layer, is placed in parallel to the PCM. This material is engineered such that it does not have an influence on the PCM while writing, but while reading the conductance state, a large fraction of the read current flows through the newly added material. The larger the fraction of the amorphous material is, the more current will pass through the projection layer. This effectively reduces the device drift and consequently lowers the drift exponent in Equation 2.7 by orders of magnitude to around $0.001 - 0.005$.

The physical reason underlying the conductance drift has been studied in literature, for example in [66, 69, 70, 71]. It is commonly agreed that the root cause is a spontaneous structural relaxation ongoing in the amorphous state of the PCM. This is because melt-quenching, as described above, is used to create the amorphous state. In this procedure the atoms in the liquid phase are cooled rapidly and essentially freeze in place, without the chance to reach an ideal glass state. In the following, a relaxation process is ongoing to bring the system into the energetically

more favorable ideal glass state. One model that can be used to describe this process, which is also in good agreement with the observed behavior, is considering a collective rearrangement of defects in the amorphous state. At the heart of this model is the physical picture that the glass state created during melt-quenching is an unstable state which eventually traverses through a series of collective transitions, with an associated activation energy, to the ideal glass state.

Noise in PCM materials

The second fundamental problem of PCM devices is the special type of noise they exhibit, which is different from the common Johnson noise known in electrical resistors. In these devices, 1/f noise can be experimentally observed [65, 72, 73, 74]. Both, the low-frequency noise and the previously described conductance drift are especially relevant applications of PCM devices, because these effects impose constraints on how frequently and how precise the state of the cells can be retrieved. It can be observed that the 1/f noise is detrimental for PCM-based in-memory accelerators, as it limits the precision with which the cells can be programmed and consequently the precision with which operations can be carried out. Moreover, 1/f noise is observed in both states, in the amorphous RESET state as well as in the polycrystalline SET state. Although, the magnitude of the noise is orders of magnitude lower in the polycrystalline state, this may still indicate that the underlying physical mechanism is the same in both states.

One important parameter of the 1/f noise is the slope exponent γ, as given in Equation 2.6. In ideal 1/f noise, this slope exponent is equal to one as can be seen in Figure 2.1, but in real devices it may differ. For example in PCM devices, the slope exponent can range between $0.9 - 1.1$ [75, 76, 77, 78], whereas values ≥ 1 are observed for the polycrystalline SET state and values ≤ 1 are observed for the amorphous RESET state. In addition to the state dependency, experiments show that the amplitude of the noise is also dependent on the voltage used for the reading as well as on the ambient temperature [75, 79].

Because the understanding of low-frequency noise is at the heart of this thesis, the entire Chapter 3 is devoted to investigate theoretical models from literature and to devise a strategy of how to get more insights into the underlying physical phenomenon.

3
Low-frequency noise

In contrast to the conductance drift phenomenon, which is well-studied, there is not a large body of literature dealing with theories that underly the low-frequency noise in PCM devices. Moreover, the relevant literature works date back many years and a commonly agreed theory is still missing. Firstly, this chapter aims to summarize the background from literature about the origins and properties of 1/f noise in a wide variety of materials. Afterwards, the literature specifically investigating low-frequency noise in chalcogenide glasses will be reviewed.

As already outlined in Section 2.1.2, the first observations of the low-frequency noise were documented in the early 20th century by Johnson [29]. Early experiments were carried out on metal films made from different materials and the noise spectra was measured at room temperature or above. Although there were results reported on noise measurements carried out under cryogenic temperatures, created with liquid nitrogen or even liquid helium, these results were potentially erroneous and were disregarded in later studies [80]. When the low-frequency noise was first observed, it was believed that it is a bulk phenomenon and originates from mobility fluctuations of the charge carriers. However, this theory is still under debate today and there is only little common agreement among different groups as we will see throughout this chapter.

One of the earliest theoretical approaches was proposed by McWhorters [81]. In his PhD thesis, he analyzed the 1/f noise in thin Germanium samples and proposed that the 1/f noise originates from charge carrier traps near surfaces and interfaces, which stands in contradiction to the belief that 1/f noise is a bulk phenomenon. In this model, the charge carriers get trapped and de-trapped, which results in a fluctuation of the number of free charge carriers. This then translates into a fluctuation of the measured current.

More than a decade later, Hooge performed noise measurements on gold films and concluded that the 1/f noise is not a surface effect [23, 24, 82], which was controversially discussed in a later letter [83]. He conducted an effort to analyze the available experimental data on 1/f noise at that time and proposed an empirical formulation

$$\frac{S_I}{I^2} = \frac{\alpha_H}{fn},, \tag{3.1}$$

where α_H is the Hooge parameter, estimated to be roughly $2 \cdot 10^{-3}$, S_I is the current noise spectra, I is the DC current flowing through the device, n is the number of charge carriers in the sample and f is the frequency. Together with further studies [84, 85] it was again suggested that a bulk phenomenon, more precisely fluctuations of the carrier mobility, is the source for the 1/f noise.

In subsequent works, this empirical formulation provided good agreement with experimental observations of 1/f noise at room temperature, but there was no theoretical justification underlying this relation or its constant α_H. Furthermore it was found that α_H could take on values different from $\alpha_H = 2 \cdot 10^{-3}$, for example Vandamme [86] measured and tabulated values of α_H from different materials. In his experiments, α_H varied roughly between $1 \cdot 10^{-3}$ and $7 \cdot 10^{-3}$. Nevertheless, the empirical Equation 3.1 is often used, even until today, to characterize the observed 1/f noise. For example, if a theoretical model for a noise source predicts a Hooge

parameter well below $2 \cdot 10^{-3}$, e.g. $\alpha' << \alpha_H$, this source is said not contribute significantly to the overall observed 1/f noise.

Over the next decades, several theories were developed with the aim to describe the physical mechanisms that could potentially cause the 1/f noise spectra. Voss and Clarke [80] revisited the experimental data acquired by Hooge and suggested a theory based on equilibrium temperature fluctuations to model the 1/f noise for continuous metal films. In their model, a temperature fluctuation ΔT results in a fluctuation of the observed voltage according to $\Delta V = IR\beta\Delta T$, where I is the current flowing through the resistor, R is the resistance value, β is the temperature coefficient and ΔT is the temperature fluctuation. The authors then argue that under certain circumstances, this voltage fluctuation can be observed as the 1/f noise.

Dutta and Horn [87] proposed in their work, after yet another review of the existing literature on 1/f noise, that random transition processes could be the potential source for the physical phenomenon. In particular, their theory is built on a thermally activated process with a characteristic time τ which results in a Lorentzian spectra according to $S(\omega) = \frac{\tau}{\omega^2\tau^2+1}$. Based on the findings from Bernamont [88] that if the characteristic times τ exponentially depend on some activation energy E which is uniformly distributed over a certain range according to $D(E)$, then a 1/f noise spectra emerges. Although the observed noise spectra can be explained with this model, one now has to justify the energy distribution and the thermally activated process. To this end, Dutta and Horn elaborated an energy distribution $D(E)$ that contains a single peak whose position and shape depends on the material under investigation. As we will see, this model was also picked up by later studies with different candidate distributions. Dutta and Horn also predicted that for the 1/f noise to be physically realistic, there must exist so-called frequency roll-offs. These roll-offs are areas, where the slope of the observed spectra flattens out at sufficiently low frequencies ($\gamma << 1$), respectively becomes very step at sufficiently high frequencies ($\gamma >> 1$). The authors argued that these areas are required to exist in order for the signal to contain a bounded amount of energy. A problem with these roll-offs is however, that at the low-frequency end they are hardly observed, because they are well below 1Hz and the measurement time for these frequencies becomes very difficult to handle. On the other hand at the high-frequency side, the roll-offs are hidden in the noise floor which may arise from other components of the circuitry, see Figure 2.3.

One novel and somewhat unconventional effort to describe the low-frequency noise across many different domains has been undertaken by Bak et. al. [89]. The authors suggest that there is a common underlying mechanism, called self-organized criticality. In this concept, any dynamical system with spatial degrees of freedom will evolve into self-organized critical structures. This definition of a system is very broad and covers physical systems as well as biological systems and even social sciences. A simple example of a self-organized critical structure is a pile of sand with the right slope angle or a system of interconnected pendulums. If the system is perturbed slightly, for example more sand is added, or the slope is changed, this perturbation propagates across all length scales which in turn leads to the perturbation being propagated across all time scales, resulting in 1/f noise. Although this concept is interesting as it targets illustrative examples and received great interest in many different fields of research, it has not been supported by great experimental evidence and did not make detailed predictions of the physical origin of the mechanism, respectively the observed 1/f noise [90].

In a later review study done by Weissman [90], the empirical model from Hooge was largely ruled out based on more experimental data. In addition to that, the authors mentioned that in order to satisfy the Hooge approach, the fluctuations have to occur on each carrier independently because of the factor $\frac{1}{N}$, see Equation 3.1. Based on similar argumentations, the authors also ruled out the earlier discussed equilibrium temperature fluctuation model proposed by Voss and Clarke. However, the authors concluded that many cases of the observed 1/f noise arise from

superpositions of a Lorentzian spectra, an idea which was first described by Dutta and Horn, as mentioned above. The authors claim that the noise of semiconductors can almost certainly be attributed to charge trapping/de-trapping processes which can be modelled by such a system. In addition, also in the case of metals, although much less conclusive, there also seems to be some evidence that support this model.

After a couple of years Hooge picked up this topic again and revisited the debate about the physical origin of the 1/f noise [91]. In this work, it is argued that 1/f noise is resulting from a fluctuation in the conductance value with conclusive experimental evidence. However, when it comes to the principles causing this fluctuation there is still an ongoing debate without any conclusion. The reason is that the conductance fluctuation of a sample may be caused by a fluctuation of the number of charge carriers or by a fluctuation of their mobility, as can be seen in the following formulation:

$$\sigma = nq\mu_q \tag{3.2}$$

$$\sigma_{\Delta n} = \Delta nq\mu_q \tag{3.3}$$

$$\sigma_{\Delta\mu_q} = nq\Delta\mu_q \tag{3.4}$$

where q represents the charge of the charge carriers, n represents the number of charge carriers and μ_q represents the mobility of the carriers. The fact that the noise can be observed in bulk samples, in gold films and later also in other electronic devices, such as MOSFETS and BJTs [25], added even more uncertainty. To address this issue, Hooge discussed multiple theories possible sources for Δn and $\Delta\mu$, which deal with a fluctuation in the number of free charge carriers and a fluctuation in the mobility of the charge carriers respectively. While all the discussed Δn models are based on the addition of trapping mechanisms that leads to 1/f noise, similar to the Dutta and Horn model, the $\Delta\mu$ models are based on theories around charge carrier scattering. The conclusion of this work was that the 1/f noise is present in all semiconductors where the empirically found Hooge relation holds. Another important observation was that the magnitude of the 1/f noise is smaller in a perfect crystal compared to a material where the crystal structure was damaged. The increase in noise was found despite the fact that the mobility of the charge carriers only hardly changed. However, it was also concluded that it is not clear, whether the noise is caused by bulk effects or surface effects. Finally, it was suggested that a combination of both effects is the potential source for the low-frequency noise.

All the above-mentioned theoretical studies along with the experimental findings suggest that there are multiple potential sources for 1/f noise. In addition, they were performed on continuous metal films or on semiconductors, where the 1/f noise was often observed on top of the common thermal noise. This clearly suggests that the phenomenon behind the 1/f noise is not unique for chalcogenide glasses and there are commonalities. Due to the increasing popularity of chalcogenide glasses, two research groups picked up the topic of 1/f noise a couple of years later. Therefore, in the remainder of this section we will focus specifically on theoretical models and experimental studies of 1/f noise for PCM devices.

The first group is formed around Fantini, which published one of their first papers about 1/f noise in chalcogenide glasses in 2006 [73]. This work was experimentally oriented and geared towards measuring 1/f noise in chalcogenide glasses. They found that the magnitude of the noise is dependent on whether the phase-change material is in the polycrystalline or the amorphous state, which is in-line with the findings from the previous theoretical studies. Despite the fact that the precise experimental setup they used is not well described, the authors report a Hooge parameter $\alpha_H = 10^{-4}$ which, although lower than originally suggested by Hooge, is in agreement with other values obtained for polysilicon. In addition, it is claimed that the noise cannot be

solely a result of mobility fluctuations.

The second group investigating 1/f noise is formed around Nardone [74], described many different mechanisms that are responsible of producing 1/f noise based on conductance fluctuations. These potential mechanisms include mobility and concentration modulation mechanisms, similar to [91], which are based on a two-level system (TLS), or also called double-well potential (DWP), similar to Dutta and Horn [87]. A DWP is a certain energy configuration where two minima at approximately the same energy exist that are separated by a energy barrier. Figure 3.1 schematically depicts such a configuration. The concept of the DWP model was already

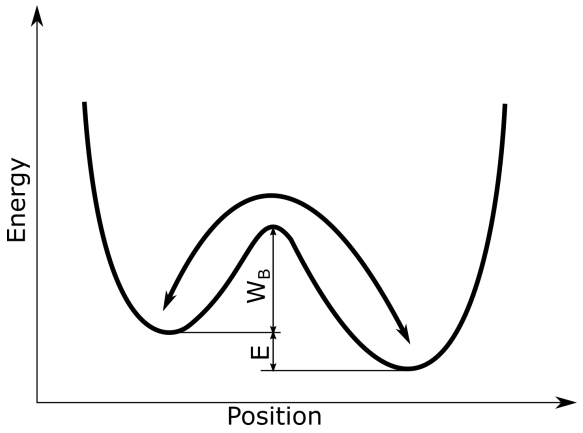

Figure 3.1: ***Illustration of a double-well potential.*** *The object in the DWP can overcome the energy barrier, it can move between the two energy minima resulting in a specific time constant τ.*

used to explain the conductance drift phenomenon present in PCM devices [92] and Nardone et. al. suggested to also utilize this model for the 1/f noise. This DWP can emerge for single atoms or a group of atoms. An illustrative are molecules, where one atom can have two minimal energy states at different bonding angles. The special property of the DWP is that if the atom has enough energy to overcome the barrier, it can switch between the two minima. The transition is a thermally activated process and leads to a characteristic relaxation time depending on the barrier height and the temperature according to

$$\tau(W_B) = \tau_0 \mathrm{e}^{(\frac{W_B}{k_b T})}, \tag{3.5}$$

with τ_0 the initial attempt rate, W_B the height of the energy barrier, k_b the Boltzmann constant and T the temperature. These transitions result in noise in the form of a Lorentzian spectrum. In a real material, many such DWP may coexist with a different configuration of the position of the energy minima and the barrier heights. Essentially, the this leads to a distribution of energy barriers $W_{B,min} < W_B < W_{B,max}$ and respectively to a superposition of many individual transitions resulting in an exponentially broad distribution of time constants $\tau(W_B)$. This superposition of many Lorentzian spectra effectively causes a 1/f spectra to emerge [93]. A more in-depth discussion about the DWP model can be found in [87, 94]. In addition to the atomic DWP, the authors also investigated the electronic structure of chalcogenide glasses. They reviewed experimental data of noise in chalcogenide glasses and observe that there are two classes, one showing experiments in favor of a high density of localized states and a second one showing experimental evidence for a low density of localized states. This discrepancy was already investigated by Anderson to explain the anomalies of the specific heat, the thermal conduction and other properties in glasses at low temperatures [95]. As a result, he suggested a so-called negative Hubbard model, negative-U model, to resolve this problem [96]. In this model a state where two electrons (2e) or two holes (2h) are in one state is energetically more favorable

compared to a singly occupied state (1e/1h). Nardone et. al. propose the negative U-model to be the source of an electronic DWP, where the two minima are formed by states of (2e/2h) and (0,0). All of the findings of this work are then later summarized and published in the PhD thesis of Nardone [97].

At a similar time, the DWP model was also used to explain the RTN observed in the intermediate states of PCM devices, see Section 2.1.2. The characteristic transition times from the lower level to the higher level τ_{12} and vice versa τ_{21} were modelled as two energetically similar minima that are separated by an energy barrier. It was observed that these characteristic times were distributed according to a Poisson distribution [35].

In subsequent works, Fantini and his colleagues developed a numerical model that could explain their observed noise behavior [75, 79]. The authors argue that fluctuations of the mean trapping energy of the material translate into fluctuations of the number of the free charge carriers and eventually into fluctuations of the conductance which can be observed as 1/f noise. Their physical model is also based on the DWP described above but does not utilize the negative-U model. Instead, they assume that each DWP system corresponds to a donor or acceptor trap. The authors in this work do not discriminate between atomic and electronic contributions, but they experimentally found that the 1/f noise in chalcogenide glasses is dependent on the bias voltage, the temperature, and the phase configuration of the PCM device. Furthermore, they used a specific distribution of number of the states depending on the barrier energy W_B of the form

$$N(W_B) = N_0 exp\left(-\frac{W_B}{E_D}\right), \tag{3.6}$$

where N_0 is some maximum value of $N(W_B$ and E_D is related to the slope factor γ of the 1/f spectrum. In particular, their model suggests that the slope factor γ can be calculated as

$$\gamma = 1 - \frac{k_b T}{E_D}, \tag{3.7}$$

which could be verified experimentally. With this the authors were able to model the experimentally observed $\frac{1}{f^\gamma}$ spectrum with a slope factor of $\gamma \neq 1$.

A final notable conclusion of this work is that the noise is said to be a bulk phenomenon rather than an interface phenomenon. More recent work from the same group builds upon their model and mainly investigate scaling effects to smaller technology nodes [98]. However, the theory is left untouched.

The presented literature research uncovered a few things around the 1/f noise. First of all, there is not an extensively large body on this topic compared to other related problems, such as the drift phenomenon. In addition to that, there are many contradicting opinions and discussions, without a widely accepted theory about the origins of the 1/f noise of metals and especially of chalcogenide glasses. For example, the only agreed fact found so far is that 1/f noise is caused by conductance fluctuations, but whether these are caused by bulk effects like fluctuations of the carrier mobility, or whether these are caused by surface traps affecting the number of charge carriers, is still unclear. Despite this, one can see certain similarities in the recent research efforts on chalcogenide glasses with the previous efforts for metals and semiconductors. In particular, the DWP model regained a lot of attention and is used in the latest approaches of the group around Nardone and Fantini. Since this model was also very popular due to the work of Dutta and Horn and was also used to explain different, but related mechanisms like the conductance drift, it appears to be a promising theoretical model.

Therefore, this thesis makes use of the DWP model to investigate the 1/f noise in PCM

devices. It aims to verify this model with experimental measurements on PCM devices over a large range of temperatures, which has not been done for PCM devices so far. This study of the temperature dependence is especially relevant, as there is an exponential decrease of the noise amplitude predicted, and could potentially yield new insights into the noise behavior of PCM devices, see the following simulation Chapter 6 for more details.

4

Theoretical model

The theoretical model used in this thesis is inspired by the DWP concept put forward in [74, 87, 95]. As explained in the previous chapter, the essence of this model is that there are two slightly different energetic minima, separated by a barrier of height W_B. An object in this system can move from one minimum to the other with a certain characteristic time which can be described as

$$\tau = \tau_0 exp\left(\frac{W_B}{k_b T}\right), \tag{4.1}$$

with τ_0 the initial attempt rate, k_b the Boltzmann constant and T the temperature. The initial attempt rate was related to the atomic vibrations by Nardone and estimated to be 10^{-13} s. A similar value of 10^{-14} s was assumed by Dutta and Horn. This transition is considered to be a random process with a characteristic transition time τ which results in a Lorentzian spectrum with the PSD

$$S(f,\tau) = \frac{N_0\tau^2}{1+\tau^2 f^2}, \tag{4.2}$$

where N_0 is a constant prefactor. The assumption in the DWP model is that there are many of these systems in a material with different configurations, e.g. the W_B is distributed according to some distribution $D(E)$. In addition, Hooge emphasized in one of his works, that it is important that the individual DWP systems are isolated. This means that for a 1/f spectra to arise, there should be no transition from a DWP with τ_1 to a DWP with τ_2.

If we assume that these conditions are satisfied then one can integrate over many individual Lorentzian spectra 4.2 and one obtains

$$S(f) = \int S(f,\tau)D(\tau)d\tau, \tag{4.3}$$

which, after a transformation of the integration variable from τ to W_B becomes

$$S(f) = \int S(f,\tau(W_B))D(W_B)\frac{\mathrm{d}W_B}{\mathrm{d}\tau}\mathrm{d}\tau \tag{4.4}$$

$$= \int S(f,\tau(W_B))D(W_B)\frac{k_b T}{\tau(W_B)}\mathrm{d}W_B \tag{4.5}$$

$$S(f) = \int \frac{N_0\tau(W_B)}{1+\tau(W_B)^2 f^2}D(W_B)k_b T\mathrm{d}W_B \tag{4.6}$$

As explained in [87], the task is now to motivate suitable distributions of the energy barrier $D(W_B)$. There have been a few candidates proposed in literature, which are a uniform

distribution [87], an exponentially decreasing distribution [79] and a peaked distribution [87]:

$$D(W_B)_{uni} = \frac{1}{W_{B,max} - W_{B,min}} \tag{4.7}$$

$$D(W_B)_{exp} = exp\left(-\frac{W_B}{E_D\left(\gamma, T\right)}\right) = exp\left(-\frac{W_B(1-\gamma)}{k_b T}\right) \tag{4.8}$$

$$D(W_B)_{peak} = \frac{1}{\sqrt{2\pi 0.4}} exp\left(-\frac{(W_B - 1)^2}{2 \cdot 0.4}\right) \tag{4.9}$$

$$\tag{4.10}$$

The factor E_D in the exponential distribution links the energy distribution with the slope factor $\gamma = 1 - k_b T E_D$. This equation was observed in some PCM devices and also presents a valuable parameter for this thesis, as it depends on temperature and can be verified experimentally. However, this expression is problematic, because if the slop factor is equal to 1, then E_D diverges. This means that the observed low-frequency noise is never exactly a pure 1/f noise. The peaked distribution in the last example is of Gaussian shape with a mean of 1 eV and a variance of 0.4 eV, which was given as an example in [87]. However, it was also reported, that for different materials, this distribution might change in terms of the mean and the standard deviation. Note that in the simulation results presented in Chapter 6, the barrier distributions are normalized such that $\int_{W_{B,min}}^{W_{B,max}} \mathrm{d}W_B = 1$.

If one performs the integral in Equation 4.6 with a uniform distribution $D(E)$, one obtains

$$S(f) = \frac{k_b T}{W_{B,max} - W_{B,min}} \int_{W_{B,min}}^{W_{B,max}} \frac{N_0 \tau_0 exp\left(\frac{W_B}{k_b T}\right)}{1 + f^2 \tau_0^2 exp\left(\frac{2W_B}{k_b T}\right)} \mathrm{dW_B} \tag{4.11}$$

$$= \frac{N_0 k_b T}{W_{B,max} - W_{B,min}} \int_{W_{B,min}}^{W_{B,max}} \frac{\tau_0 exp\left(\frac{W_B}{k_b T}\right)}{1 + f^2 \tau_0^2 exp\left(\frac{2W_B}{k_b T}\right)} \mathrm{dW_B} \tag{4.12}$$

$$= \frac{N_0 k_b^2 T^2}{f \cdot (W_{B,max} - W_{B,min})} \cdot \tag{4.13}$$

$$\left[arctan\left(\tau_0 \cdot f \cdot exp\left(\frac{W_{B,max}}{k_b T}\right)\right) - arctan\left(\tau_0 \cdot f \cdot exp\left(\frac{W_{B,min}}{k_b T}\right)\right)\right] \tag{4.14}$$

$$S(f) = \frac{C}{f}\left[arctan\left(\tau_0 \cdot f \cdot exp\left(\frac{W_{B,max}}{k_b T}\right)\right) - arctan\left(\tau_0 \cdot f \cdot exp\left(\frac{W_{B,min}}{k_b T}\right)\right)\right] \tag{4.15}$$

If the term $arctan(\cdot)$ is considered to be a constant, than $S(f)$ is proportional to $1/f$ which results in the typical 1/f noise, see [87] for a similar derivation. Experiments show that in practice the prefactor is not always constant and therefore $S(f)$ might be more complex which may result in slopes with a coefficient $\gamma \neq 1$.

In the following, this theoretical model is used to fit observed noise data from real PCM devices. To this end, a MATLAB program was developed that performs a numerical integration of Equation 4.6, where $N0$ was a fit parameter. This parameter is adjusted to create a good overall fit of the predicted noise spectra by the model and the observed data.

5
Experimental setups

This chapter forms the basis for the thesis and all the following experiments. It outlines the techniques and requirements necessary to conduct the sensitive noise measurements. It is divided into three parts. First, the custom electrical circuitry required to measure low-frequency noise is described along with the calculations needed to convert the raw data into the PSD. The second part focuses on preparing the noise measurement setup at room temperature with all the subtle details one has to pay close attention to. The same process is then discussed in the third section for the setup in the cryostat.

5.1 Measurement circuitry

In order to study the low-frequency noise of PCM devices, a specifically designed measurement circuitry was used [99], which is depicted in Figure 5.1. The mushroom type PCM device used

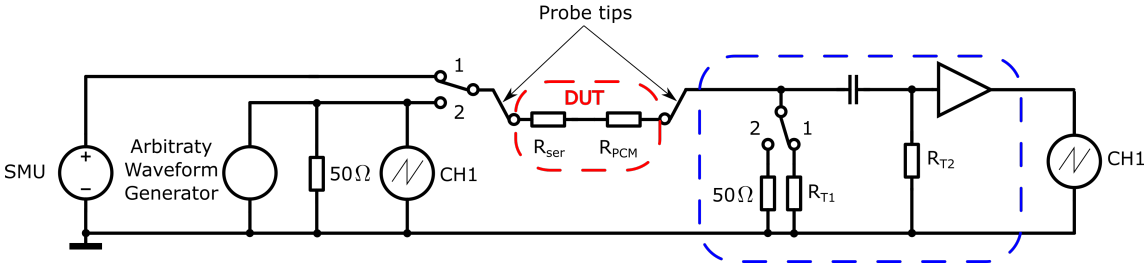

Figure 5.1: ***Circuitry used to measure the noise of a DUT.*** *The circuitry consists of two paths. One path is used to measure the noise of a DUT, in this case a PCM device, and the second path is used to program the PCM to a particular conductance state.*

in this thesis is depicted in the center and part of the 'Device under test (DUT)' whose noise behavior should be investigated. The DUT is contacted with electrical probes, as illustrated in Figure 5.1. In addition to the PCM, Figure 5.1 shows also a series resistor R_{ser} connected to the PCM that is also part of the DUT and typically integrated on the same chip as the PCM device itself. This resistor is used as a static current limitation to avoid that excessive currents flow through the PCM device, which might damage the device. For example, if the PCM device gets programmed and switches to the low-resistive polycrystalline state, R_{PCM} would become suddenly very small and the previously applied voltage across the device will cause significant currents to flow which might destroy the device permanently. The series resistor limits the current in a way that only a maximum current defined by $I_{max} = \frac{U_{bias}}{R_{ser}}$ can flow.

The circuitry itself contains two main paths, one path to measure the noise of the device, indicated by the relay configuration 1 and a second path to program the cell to a different conductance state, indicated by the relay configuration 2. The first path to measure the noise of the device includes a Source Measure Unit (SMU) that is used to bias the PCM device, the DUT marked in red, an amplifier board marked in blue and an oscilloscope. The amplifier board consists of a 50Ω resistor, R_{T1} a capacitor, R_{T2} and a two-staged operation amplifier (OP). The capacitor is used to block the DC bias voltage from the SMU during the noise measurement.

The gain G of the OPs was set to $G_1(f) = 52$ and $G_2(f) = 11$, totaling in a gain of $G(f) = 572$. The total gain was chosen in such a way that the OP board achieves a high amplification factor, while still maintaining a bandwidth of $100k$Hz. For the exact details of the OP gain calculation, the reader is referred to [99]. With these settings, the noise of the PCM device can be measured up to $100k$Hz in a variety of different conductance states with the oscilloscope (OS). It is important to mention however, that the circuitry used causes the gain $G(f)$ to depend on frequency. Especially at low frequencies, for example at 1Hz, the gain of the OP decreased if the resistors are not chosen properly. Before even measuring the noise of any individual component, the gain of the OP has been investigated, whether it remained constant given the typical configurations of the board.

The second path of the circuitry is used to program the PCM device to a different conductance state. To program the device, voltage pulses of different amplitudes and durations, generated by an arbitrary waveform generator (PG), are applied to either crystalize the PCM or to perform a melt-quenching to amorphize the material. Typical characteristics of applied pulses are listed in Table 2.1 in Section 2.2. The arbitrary waveform generator is coupled to a MATLAB script that allows to perform the state transitions automatically. In addition, the script also allows to program the device in a closed-loop scheme, called iterative programming, to a desired conductance state within a certain margin. To enable accurate shapes of the pulses, in particular fast raising edges, all the lines in the circuitry in this path have to be terminated with $50\,\Omega$ resistors to avoid any wave reflections that distort the shape of the pulse.

The procedure to measure the noise of the PCM device, is separated into three stages followed by a post-processing stage. In the first stage, the resistance of the PCM device is measured. This step is required to bias the PCM device always with the same voltage, regardless of its conductive state. In the second step, the noise of the PCM device amplified by the OP is measured with the oscilloscope multiple times to allow averaging later. As the last step, the DC current flowing through the PCM device is measured. This is done afterwards to ensure that the state of the PCM device is not altered anymore. The DC current is later used during the post-processing stage, which is performed on a computer using MATLAB, to normalize the noise spectrum. The captured noise data from the oscilloscope is transformed into the PSD using Welchs algorithm [100]. After the PSD has been calculated, known noise components arising from the circuitry itself, for example coming from the individual resistor R_{T1} or R_{T2}, as well as the noise coming from other sources like the SMU or the OP can be subtracted. Depending on the application, the final result can then be normalized using the DC current.

The different noise contributions of the individual circuit components have been analyzed in the previous work [99] and can be expressed through the following formula:

$$\begin{aligned} S_{tot}(f) = &[S_{SMU}(f) + S_{ser}(f) + S_{PCM}(f)] \left(\frac{R_{load}}{R_{load} + R_{ser} + R_{PCM}} \right)^2 G(f)^2 \\ &+ S_{load}(f) \left(\frac{R_{ser} + R_{PCM}}{R_{load} + R_{ser} + R_{PCM}} \right)^2 G(f)^2 + S_{OP}(f) + S_{OS}(f), \end{aligned} \tag{5.1}$$

with

$$R_{load} = \frac{R_{T1} \cdot R_{T2}}{R_{T1} + R_{T2}} \tag{5.2}$$

where R_{ser} and $S_{ser}(f)$ represent the resistance value and the noise of the series resistor, R_{PCM} and $S_{PCM}(f)$ represent the resistance value and the noise of the PCM cell, R_{load} and $S_{load}(f)$ represent the resistance value and the noise of the load resistor, $S_{SMU}(f)$ represents the noise

of the SMU, $S_{OP}(f)$ represents the noise spectra of the OP and finally $S_{OS}(f)$ represents the noise spectra of the OS.

If one analyzes the formula more closely, one can see that there is a relation between the load resistor R_{load} and the resistance of the PCM device R_{PCM}. Namely, if R_{PCM} is much larger than R_{load} and the noise $S_{PCM}(f)$ and $S_{load}(f)$ is on the same order of magnitude, the noise contribution from the load resistor $S_{load}(f)$ dominates and one will only measure the noise of the load resistor. In the other case, if $R_{PCM} >> R_{load}$ then one will mostly measure $S_{PCM}(f)$, but the contribution of $S_{load}(f)$ will also be higher which may have negative impacts on the final noise measurement.

5.2 Noise measurement at room temperature

Although the theory presented in Chapter 4 predicts an exponentially decreasing noise magnitude at temperatures below room temperature, this thesis first dealt with noise measurements at room temperature. The reason for doing so is because the measurement setup built for this temperature regime is simpler and more accessible, but still provides valuable contributions to a more fundamental insight into the working principles of PCM devices. Since the setup is built to operate at room temperature, it is referred to as room temperature setup in the following.

The setup for the room temperature noise measurement is shown in Figure 5.2. The wafer

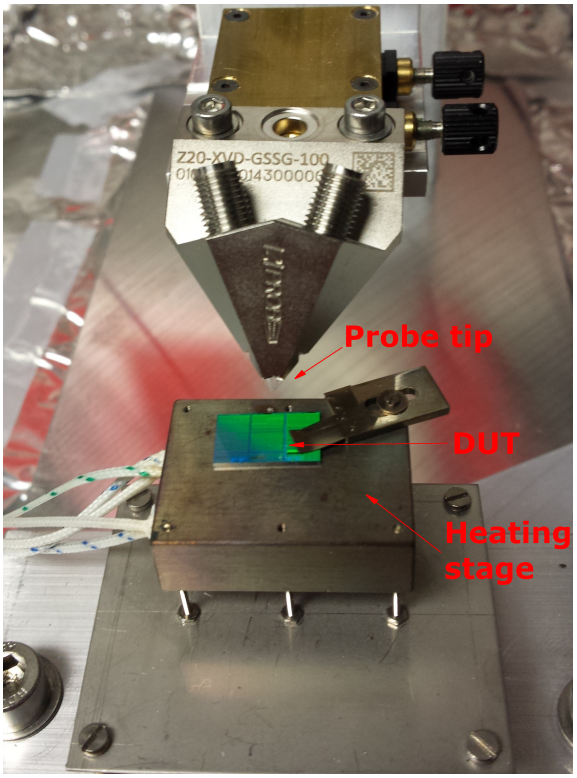

Figure 5.2: ***Noise measurement setup for room temperature.*** *Electrical probes are used to contact the PCM device directly on a pre-cut wafer. The SMU signal or the PG signal is delivered at the input of the probe (left-hand side, see circuitry in Figure 5.1), while the output of the probe serves as the input for the OP*

piece is mounted on a heating stage that can be used to perform measurements at elevated temperatures in a range roughly between room temperature and 200°C.

When building a noise measurement setup, it is crucial to investigate the individual components. Noise measurements are inherently very sensitive to distortions and to undesired influences from other noise sources. Therefore, the contributions coming from the individual circuit components needs to be understood well. To do so, the noise of every single component, starting from the OS alone, are investigated. For example, it turned out to be essential that the cable lengths of the circuitry are reduced to the minimum length. Otherwise these cables act like antennas and pick up any electromagnetic waves from the surrounding. Also the lighting sources and the particular placement of the setup caused problems, as the PWM-controlled lights as well as the close by power supply of the laboratory emitted electromagnetic distortions which were immediately picked up by the setup and lead to distortions of the measurement. To reduce these influences a Faraday cage was built to encase the entire measurement setup. The effect of this cage can be clearly seen in Figure 5.3.

Figure 5.4 shows the noise floor of the oscilloscope alone without any circuitry attached. This is the lowest possible noise one can measure. In addition to that, the PSDs of two regular resistors are shown with their theoretical value. The noise of the oscilloscope alone shows almost periodic ripples at frequencies above 50Hz which are also present in the noise spectra of the resistors. Although one might assume that these ripples have the same origin and one could remove them via post-processing, this has not been done in the results presented in the following. The main reason for this is that the source of these ripples could not have been identified accurately.

After the individual noise sources have been analyzed, the PCM device is contacted with an electrical probe directly on a pre-cut wafer as shown in Figure 5.5.

5.3 Noise measurement at cryogenic temperatures

The theory presented in Chapter 3 suggests that the noise magnitude of PCM devices is exponentially decreasing when cooled to low temperatures. This interesting phenomenon can be a key indicator whether this noise model can indeed describe the observed behavior. However, in order to achieve temperature well below room temperature, a cryostat operating under vacuum conditions is required. To achieve this, a cryostat with a liquid nitrogen cooling system is used that can achieve temperatures close to $T_{liq,N} = 77\,K$, see Figure 5.6. The cryostat consists of a vacuum chamber where the samples and the electrical probe are mounted, a liquid nitrogen cooling system to reach temperature below 100 K, as well as the same auxiliary electronic devices also used in the room temperature setup.

In order to establish a reliable platform to conduct sensitive noise experiments, all the investigations from the room temperature setup discussed in Section 5.2 need to be repeated for the individual components of this setup. Although the cryostat naturally forms a Faraday cage due to the metal casing of the vacuum chamber, there are other components that cause interferences and disturb the noise measurement. For example, the vacuum pumps that are attached to the system or more specifically, the power supplies thereof. These power supplies operate at very high frequencies and may disturb the measurement. Another source of interference is again the lighting sources of the laboratory. It can be observed that these cause distortions which shown in Figure 5.7. In contrary to the room temperature setup, this setup uses much longer cables which are required because of the manipulator of the vacuum chamber. It has already been observed in the previous setup that the cable lengths should be reduced as much as possible to avoid unintended interferences.

After all of the components have been analyzed and the ambient noise has been reduced, it is crucial to ensure that the room temperature setup and the cryostat are working reliably and yield the same results if the same device is measured. To this end, a PCM device is prepared in the room temperature setup, measured, and then immediately transferred to the cryostat. The same device is then measured at RT and the final results are compared. Figure 5.8 shows the resulting noise measurements of a RESET state measured with the two setups.

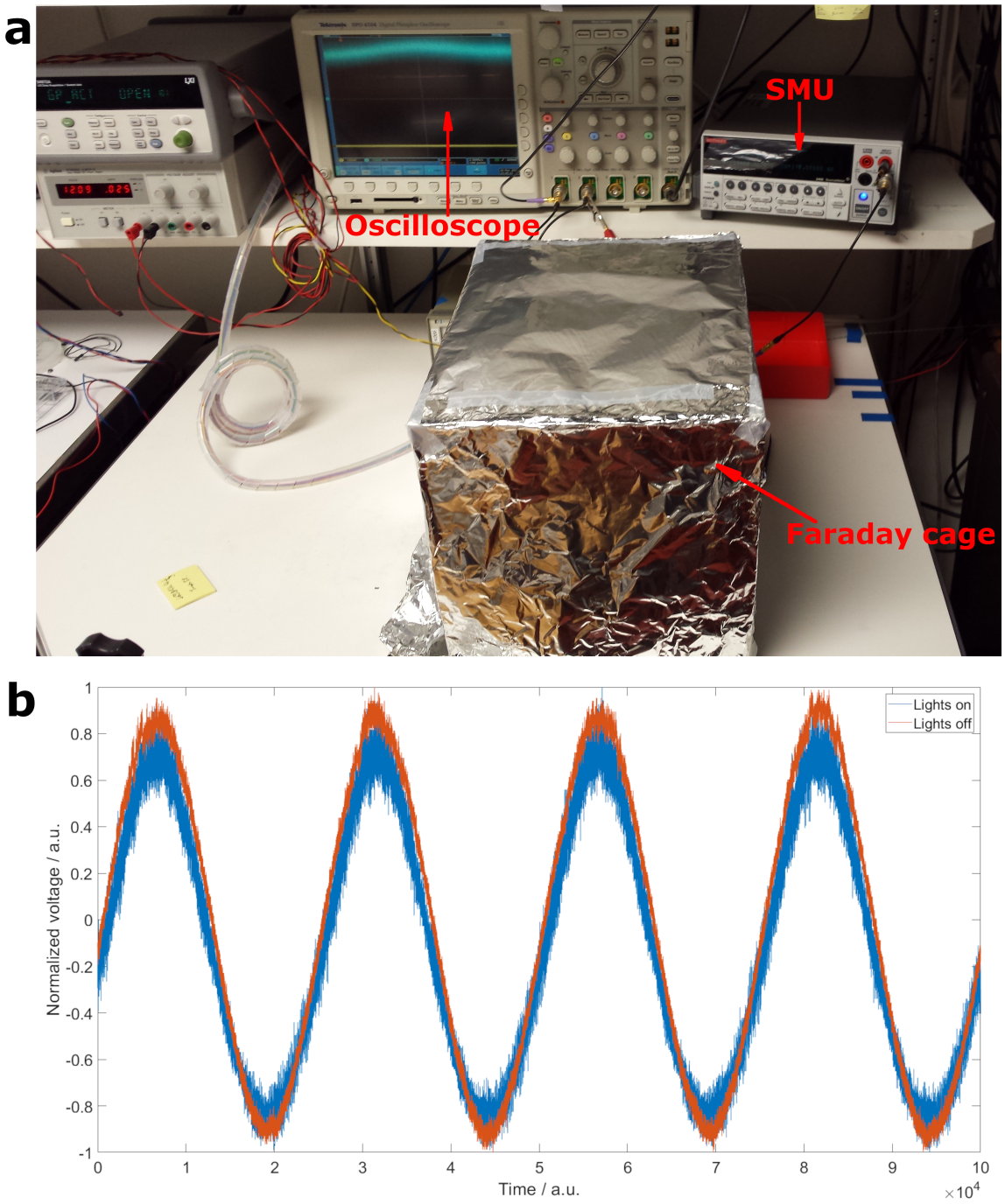

Figure 5.3: ***Faraday cage used to shield the room temperature setup.*** ***a*** *Faraday cage mounted to enclose the noise measurement setup.* ***b*** *Comparison of artificial noise signal with and without the Faraday cage. The electromagnetic are picked up by the measurement setup as distortions.* ***b*** *The Faraday cage enclosing the entire measurement setup significantly improves the quality of the noise signal.*

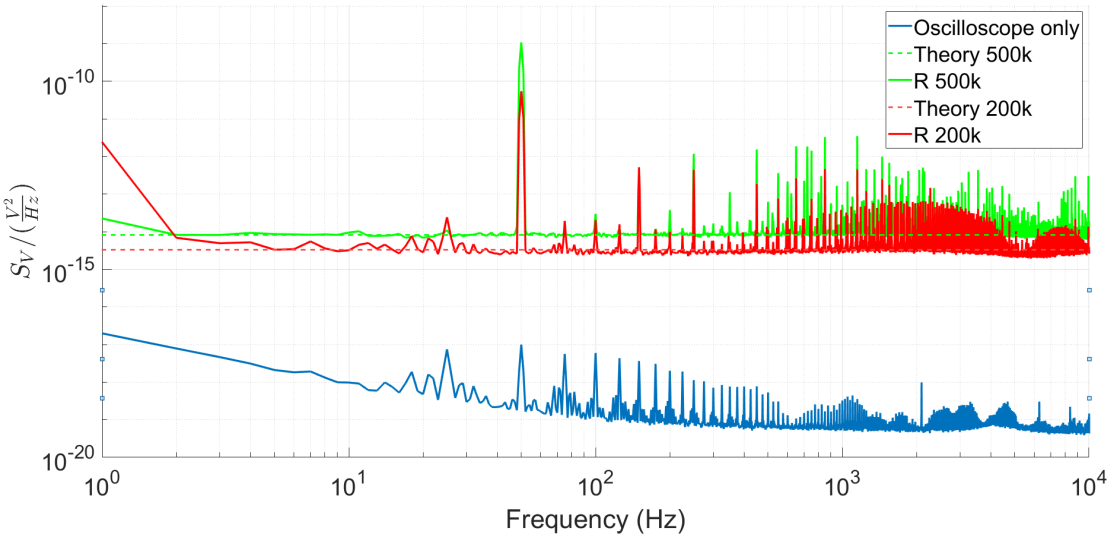

Figure 5.4: ***System noise floor and theoretical spectra.***

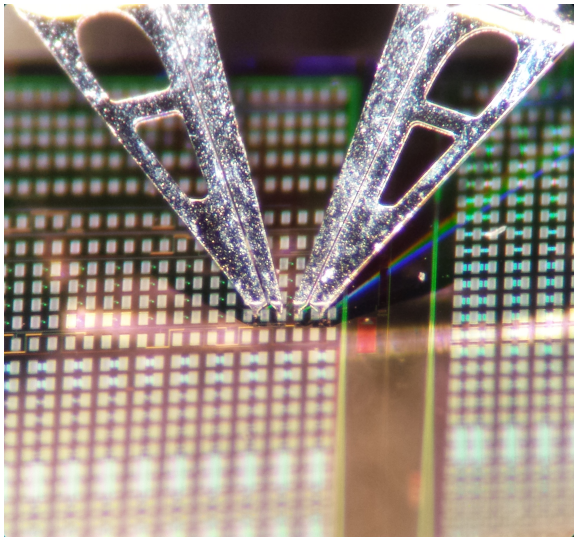

Figure 5.5: ***Electrical probes contact the PCM devices directly on a pre-cut wafer.***

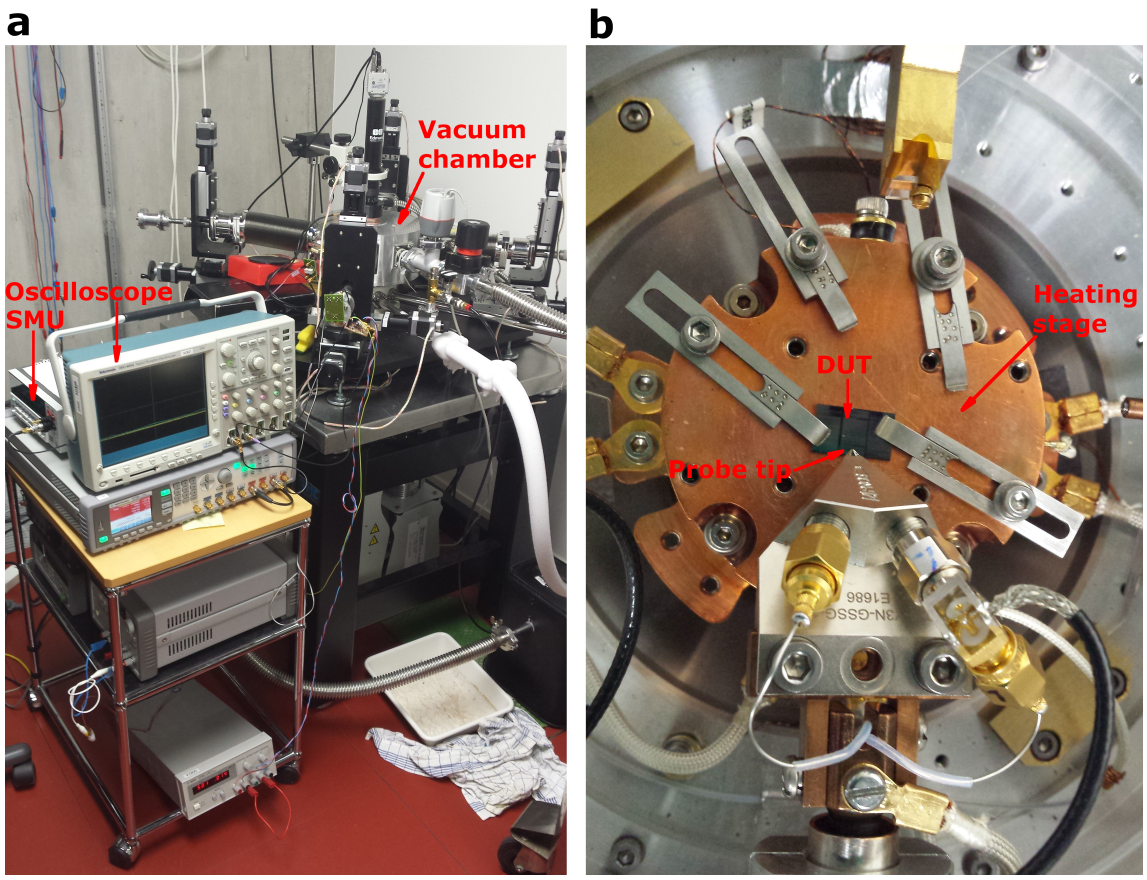

Figure 5.6: ***Cryostat used to measure low-frequency noise of PCM devices.*** *a Cryostat with vacuum pumps, cooling systems and auxiliary electrical devices. b Detail of vacuum chamber with the copper cooling block, the electrical probes and the DUT.*

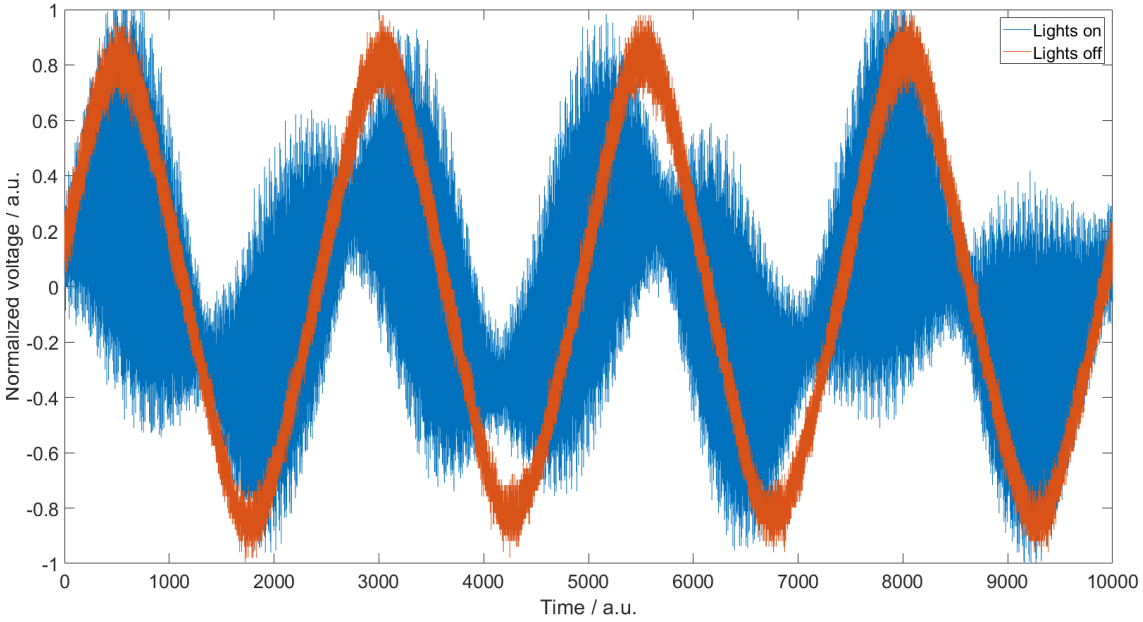

Figure 5.7: ***Influence of light sources on noise measurement setup. b*** *Comparison of artificial noise signal with lighting turned on and switched off.*

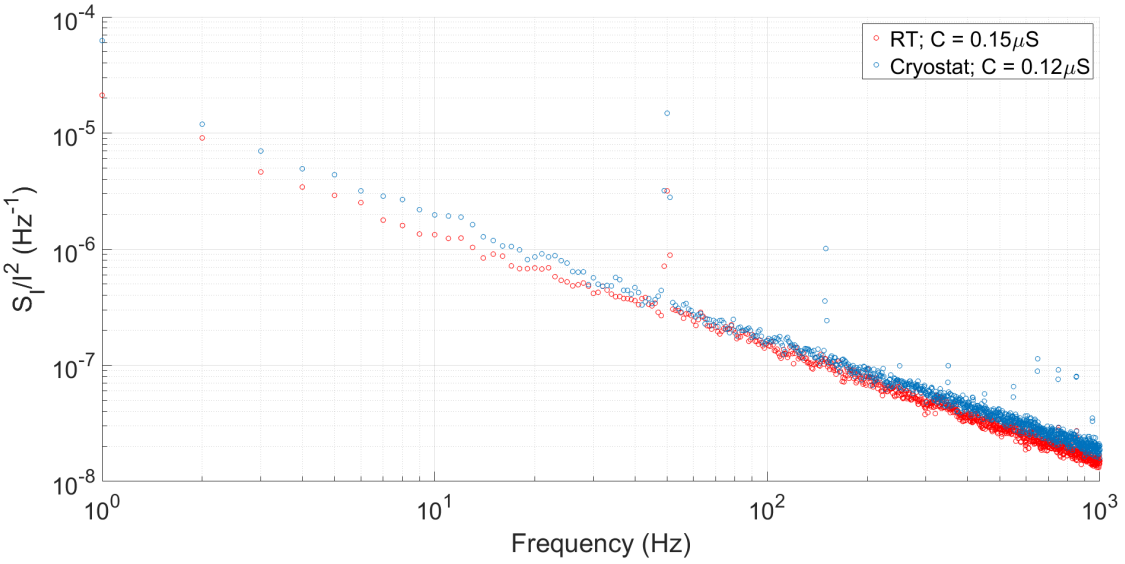

Figure 5.8: ***Comparison of noise measurements from the room temperature setup (RT) and the cryostat.***

6 Results and Conclusions

This section presents the results from the various conducted experiments. These results are accompanied with interpretations and are in addition compared to the predictions of the described theoretical model from Section 4 where possible. Furthermore, the observed trends and communalities in the results are discussed as well.

6.1 Fit of noise spectra

As a first step to verify whether the theoretical model is functional with the simplest energy barrier distribution $D(W_B)$, published noise data from PCM devices at room temperature was analyzed [68]. Figure 6.1 shows the plain 1/f noise observed in a PCM device in the RESET state.

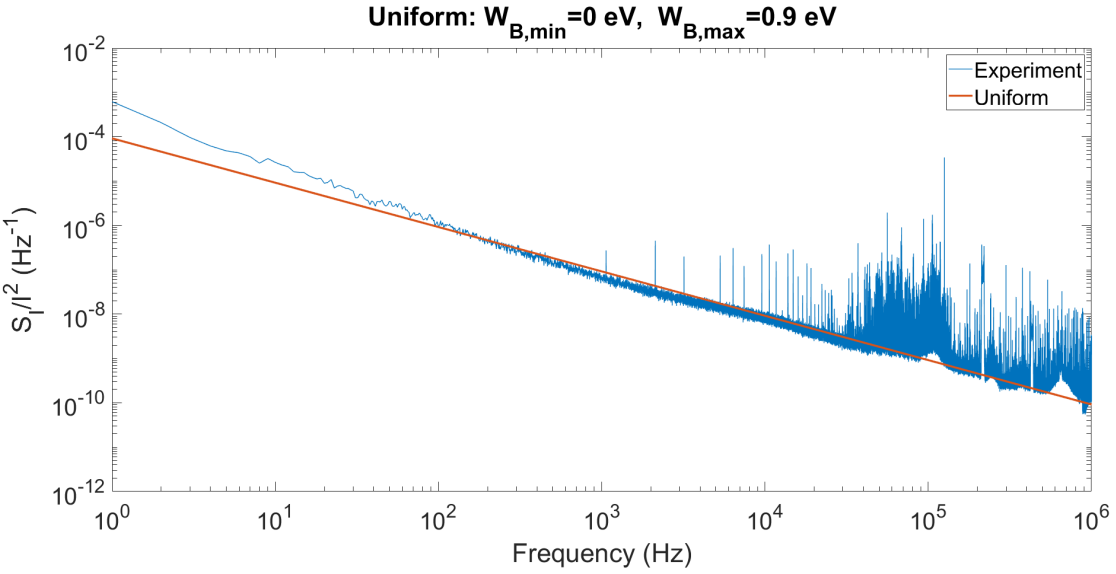

Figure 6.1: ***Normalized noise spectra of a PCM device.*** *The PCM devices was programmed in a RESET state and the noise spectra was captured at room temperature [68].*

In the next step, the model was employed fit to the data using different candidates of the energy distributions $D(W_B)$, where the used parameters are presented in Table 6.1. The results are shown in Figure 6.2. As one can see, the DWP model is able to fit the noise data reasonably well, irrespective of the energy distributions used. This is because all energy distributions give a straight line that fits the experimentally observed 1/f noise well. Since the constant prefactor is adjusted based on the measured data, the various energy distributions are able to fit the magnitude of the data as well. However, one aspect that can be observed from the different distributions is that the slope changes slightly. While the uniform distribution yields the best results with a slope close to $\gamma = 0.9$, the other two candidate distributions have a flatter slope and do not match the data that well.

Table 6.1: Simulation configuration of $D(W_B)$

Shape	$W_{B,min}$/ eV	$W_{B,max}$/ eV	Other
Uniform	0	0.9	-
Exponential	0	1.4	$\mu = 1\,\text{eV}, \sigma = 0.1\,\text{eV}$
Peaked	0	1.4	$E_D = 0.259\,\text{eV}$

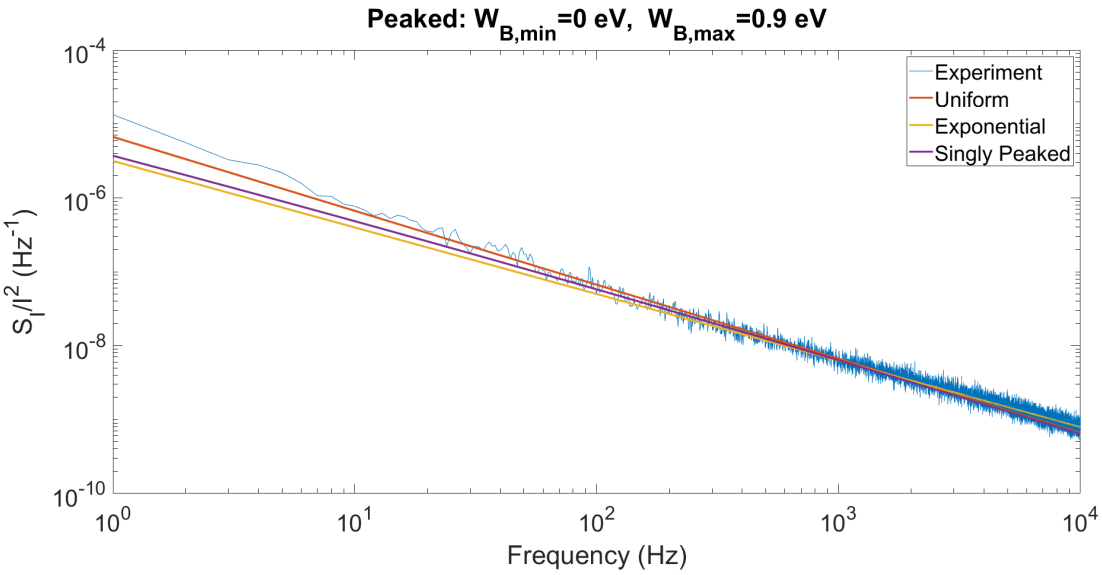

Figure 6.2: ***Fit of observed noise data with DWP model using various energy distributions*** $D(W_B)$***.***

6.2 Roll-off frequencies

At sufficiently low and high frequencies there must exist roll-offs which were predicted by Dutta and Horn as explained in Section 3. The DWP model can predict these roll-offs by limiting the allowed barrier energies to finite values. An extreme example of this is illustrated in Figure 6.3, where the lower energy bound was fixed to $W_{B,min} = 0.4\,\text{eV}$ and the upper energy bound was fixed to $W_{B,max} = 0.6\,\text{eV}$. If the lower energy bound $W_{B,min} > 0$ it causes frequency roll-offs to appear at the high-frequency end, and if the upper energy bound $W_{B,max}$ takes on smaller values, frequency roll-offs at the low-frequency end emerge.

The obtained experimental data does not show the roll-offs, neither at low nor at high frequencies, which might have two reasons. First, the roll-offs might only be visible at frequencies lower than 1 Hz, see Section 3. The problem is that experimental data on much lower frequencies might be hard to collect, as the measurement time becomes increasingly long. In addition, there are two further potential problems for the roll-offs at high frequencies. Firstly, they might not be observed because the measurement does not capture high enough frequencies (e.g. the roll-offs happen at frequencies beyond 10^6 Hz) or secondly, the roll-offs are overshadowed by the noise floor of the setup. Since the measurement data in Figure 6.3 shows a 1/f behavior over the entire frequency range, the roll-off potentially lies higher in frequency.

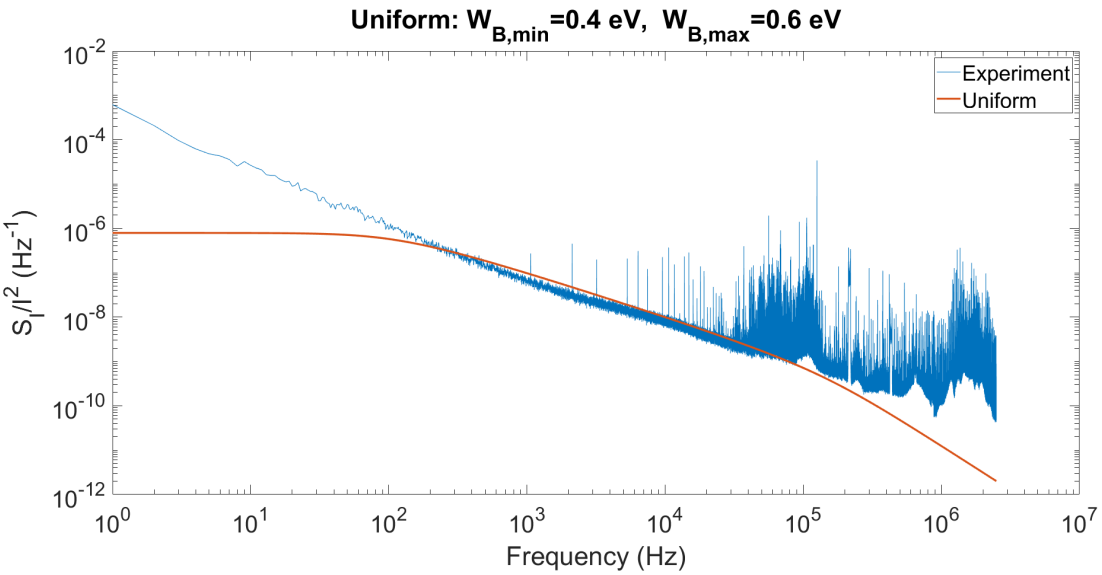

Figure 6.3: ***Frequency roll-offs predicted by the DWP with a lower barrier engery bound of*** $W_{B,min} = 0.4\,\mathrm{eV}$ ***and an upper energy barrier bound of*** $W_{B,max} = 0.6\,\mathrm{eV}$.

6.3 Noise dependence on the material composition

As explained in Section 2.2.1, the material composition of the PCM has an impact on the observed noise behavior. To study this more closely, several different material compositions, all based on GST, but with different doping concentrations, were analyzed. The low-frequency noise of these devices was investigated under similar conditions. For example, for each material, the SET state with the lowest resistance value and RESET state with the highest resistance value that could be reached with electrical pulses only was used. The observed noise for the RESET and for the SET state are shown in Figure 6.4.

In the amorphous RESET states, the atoms are highly disordered, while in the SET state, the atoms are arranged with some long-range order. Therefore, one would expect that the imperfections created by the dopants play a more important role in the SET state. This is indeed what can be observed in the 1/f noise. The noise magnitude as well as the resistance of the devices in the SET state changes much more drastically than in the RESET state. In addition, the noise magnitude in the SET shows a clear trend, gradually increasing from the pure GST to the highly doped dGST500 material.

The second observation is that the noise magnitude at 1 Hz scales with the squared resistance of the device R^2. Figure 6.5 shows the comparison of $\frac{S_I}{I^2}$ @ 1 Hz with the squared resistance R^2 of the device for both, the SET and the RESET states. One can see that the trends align well for the SET states, but the RESET states do not show such a good match. However, an interesting aspect of these results is that the scaling of the noise magnitude is present across materials. To better analyze whether the different materials show the same scaling behavior, Figure 6.6 shows the noise magnitude at 1 Hz versus the logarithm of the device resistance.

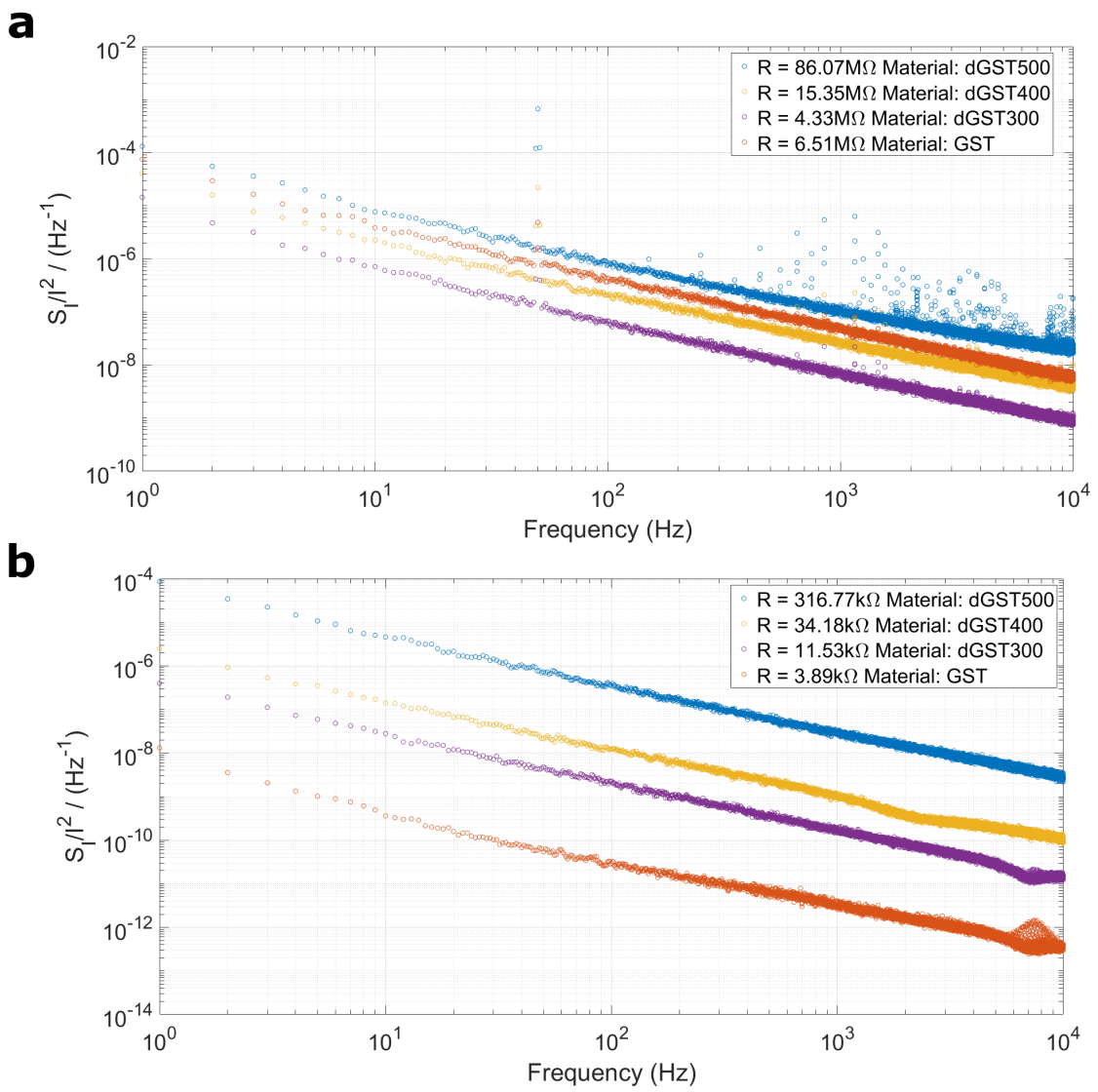

Figure 6.4: ***Influence of doping on low-frequency noise.*** *Normalized noise spectra obtained for various doping levels of GST. The devices have the same structure and the same bias voltage was applied.* ***a*** *PSDs for the RESET states.* ***b*** *PSDs for the SET states.*

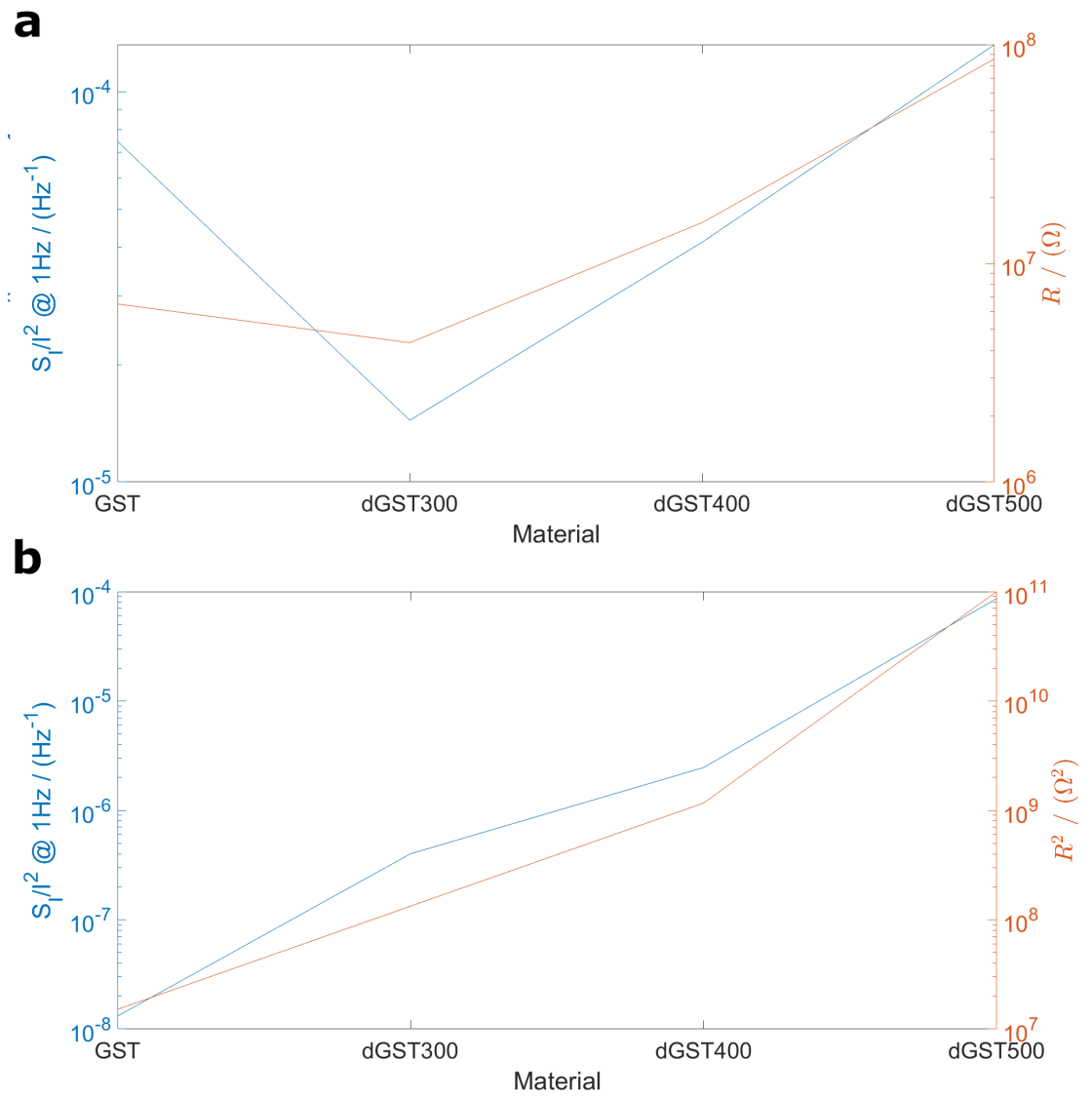

Figure 6.5: ***Comparison of the noise magnitude at*** 1 Hz ***and the resistance of different materials.*** ***a****for the RESET states* ***b*** *for the SET states.*

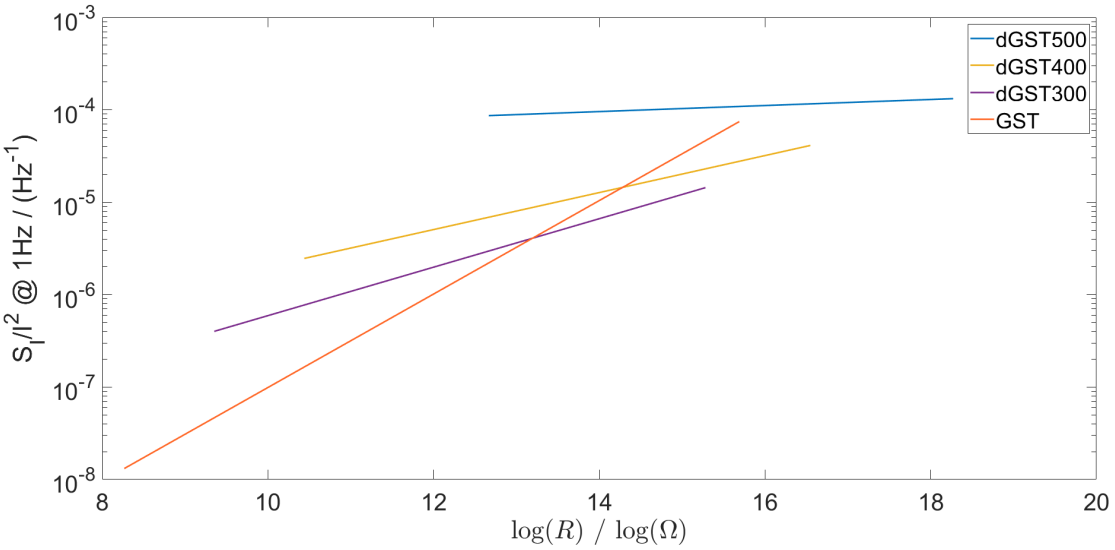

Figure 6.6: ***Noise magnitude at*** $1\,\mathrm{Hz}$ ***as a function of the logarithm of the device resistance for different materials.***

6.4 Noise dependence on the bias voltage

As explained in Chapter 2.2.7, from a technology point of view, the applied bias voltage to the PCM devices is also crucial. In general, a higher bias voltage will lead to more dissipated power and less energy-efficiency. Therefore, the aim is to use low bias voltages. However, also the bias voltage affects the low-frequency noise of the PCM device. To investigate this dependence, a doped GST PCM cell (dGST300) was measured at various bias voltages. The results for the RESET state are summarized in Figure 6.7. From Figure 6.7 one can see that the observed

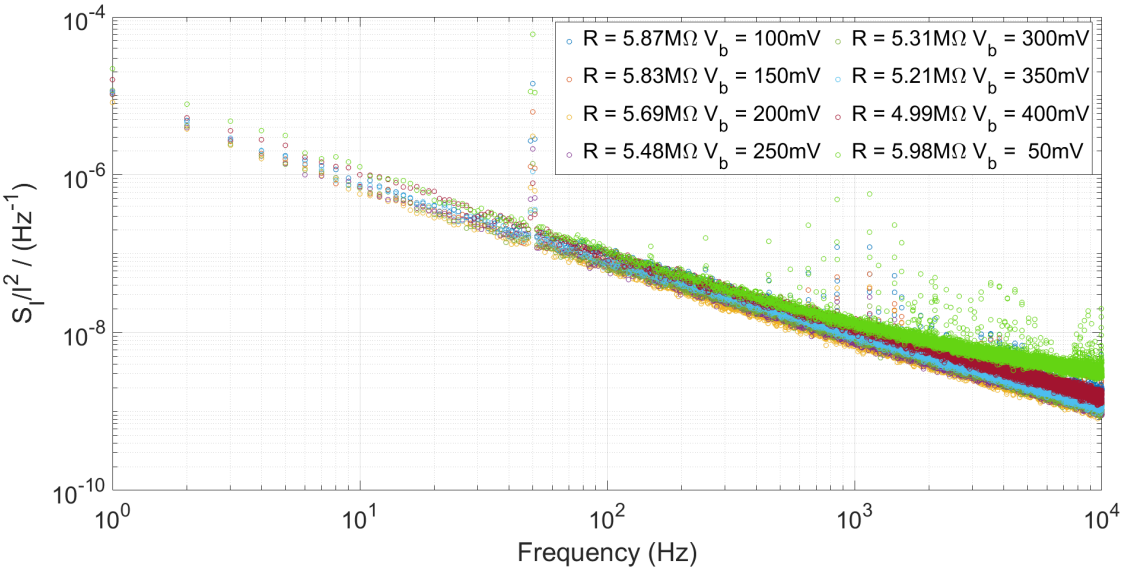

Figure 6.7: ***Noise spectra of a dGST300 PCM device under various applied bias voltages for the RESET state.***

noise is overlapping substantially, irrespective of the applied bias voltage. This behavior is very beneficial for building PCM-based chips, because the bias voltage can be reduced to low levels, without compromising on the precision of the device.

The same experiment was repeated for the SET state and is summarized in Figure 6.8. Compared to the RESET state, the noise of the SET state shows a different behavior. It can be observed that the magnitude of the 1/f noise increases as the applied bias voltage is decreased. This behavior is not beneficial from a technology point of view, as it set a lower bar on the bias voltage that has to be used for PCM-based chips. This is because if the bias voltage is decreased too far, the noise increases a lot which might result in a lower overall precision of the device. One can clearly see that although the very same state of the PCM device was just measured with different applied bias voltages, the resistance is changing. The reason for this behavior might be the nonlinear I-V behavior of the device. To verify this, the I-V curve together with the R-V curve of the device in the SET state is illustrated in Figure 6.9. This figure shows a voltage sweep of the SMU, while the current and the resistance where measured. The two curves show an upwards sweep (blue curve) and a downwards sweep (light blue curve). Ideally one would expect that the resistance of the device is constant across a large range of bias voltages. However, in the polycrystalline SET state, the PCM device has a very narrow voltage regime with an ohmic response and the applied bias voltages in this experiment are already too large, so that the non-ohmic regime is entered. As one can clearly see in Figure 6.9b, the resistance changes drastically with the applied bias voltage.

This change of the resistance might be the reason for the higher observed noise magnitudes. Figure 6.10 shows a comparison of the PSD at 1 Hz to the squared resistance of the SET state. The magnitude of the quantity $\frac{S_I}{I^2}$ can change because of a changing resistance or because of

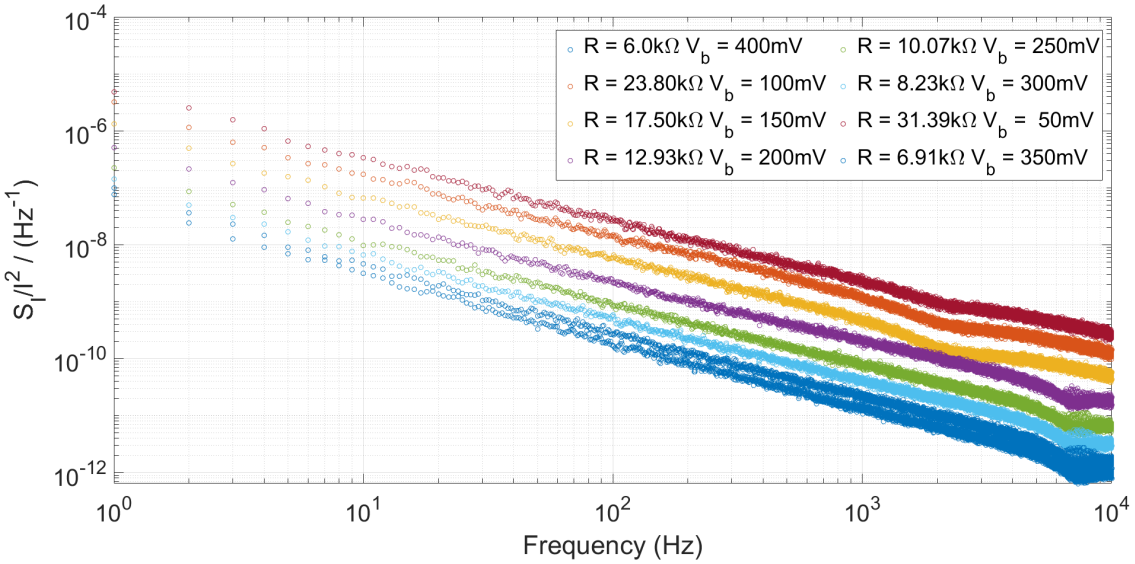

Figure 6.8: ***Noise spectra of a dGST300 PCM device under various applied bias voltages for the SET state.***

a changing current. To investigate in more detail which effect is responsible for $\frac{S_I}{I^2}$ to change, these two effects need to be decoupled. To this end, the non-normalized noise was additionally analyzed as a function of the bias voltage. If S_I is proportional to the bias voltage U^2, then this would indicate that indeed the changing resistance is causing the noise magnitude to change. Figure 6.11 shows the non-normalized noise as a function of the squared bias voltage. As one can see, S_I is proportional to U^2 and therefore the changing resistance of the device may cause the noise magnitude to change.

There are at least two potential effects in PCM devices that could cause the resistance to change. The first one is the nonlinear dependency on the bias voltage as explained above. The second one, is the temperature dependence of the resistance, as discussed later in Section 6.6. In this particular scenario, the bias voltage is high enough to cause self-heating in the device which raises the local temperature to very high values. Therefore, the resistance of the device also decreases. In addition, this effect is also the reason for the hysteresis present in the I-V and R-V curve show in Figure 6.9. Both dependencies affect the resistance of the device and therefore might change the magnitude of the 1/f noise.

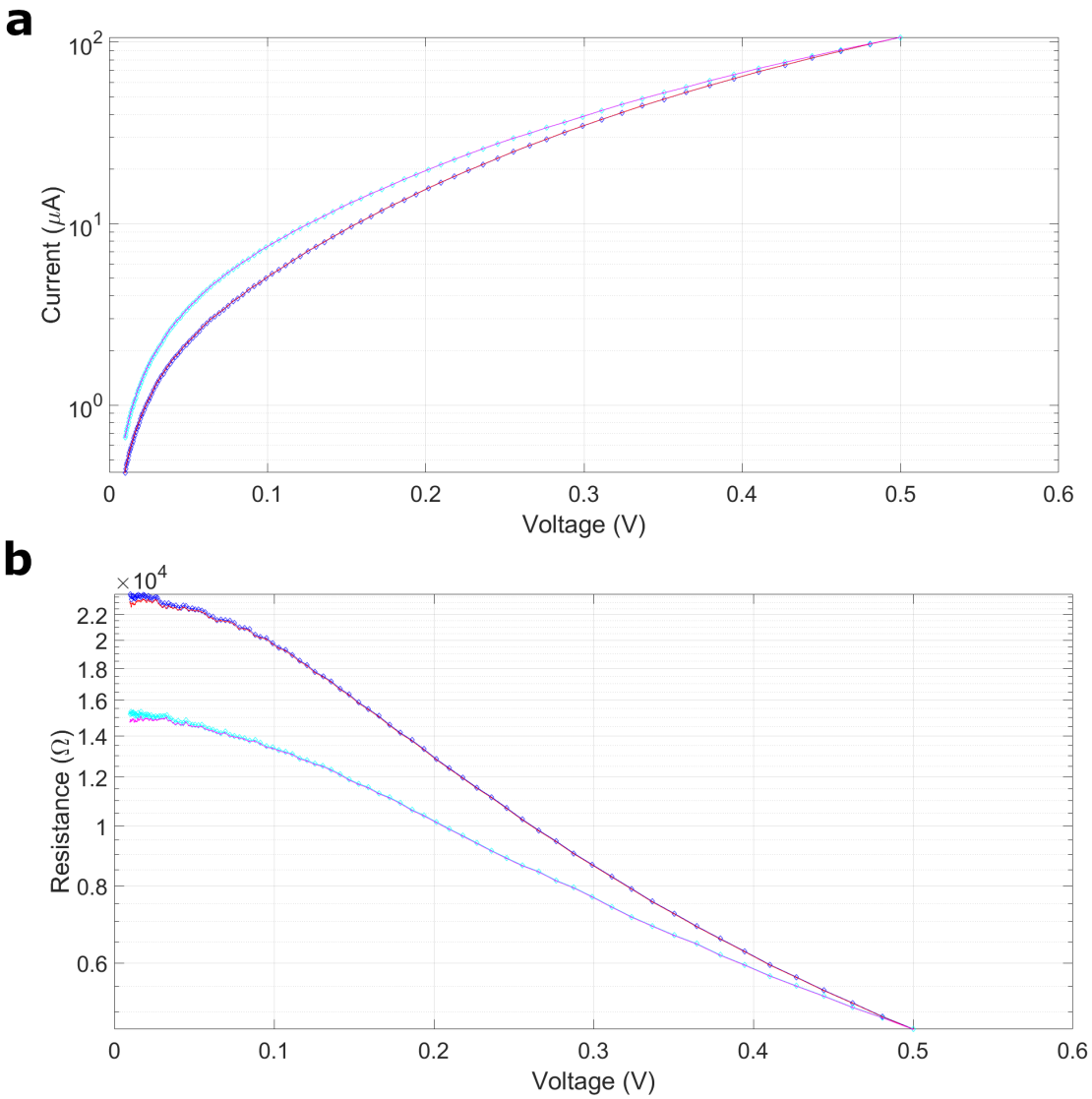

Figure 6.9: ***Investigation of the SET state of a dGST300 PCM device. a*** *I-V curve of the device.* ***b*** *R-V curve of the device.*

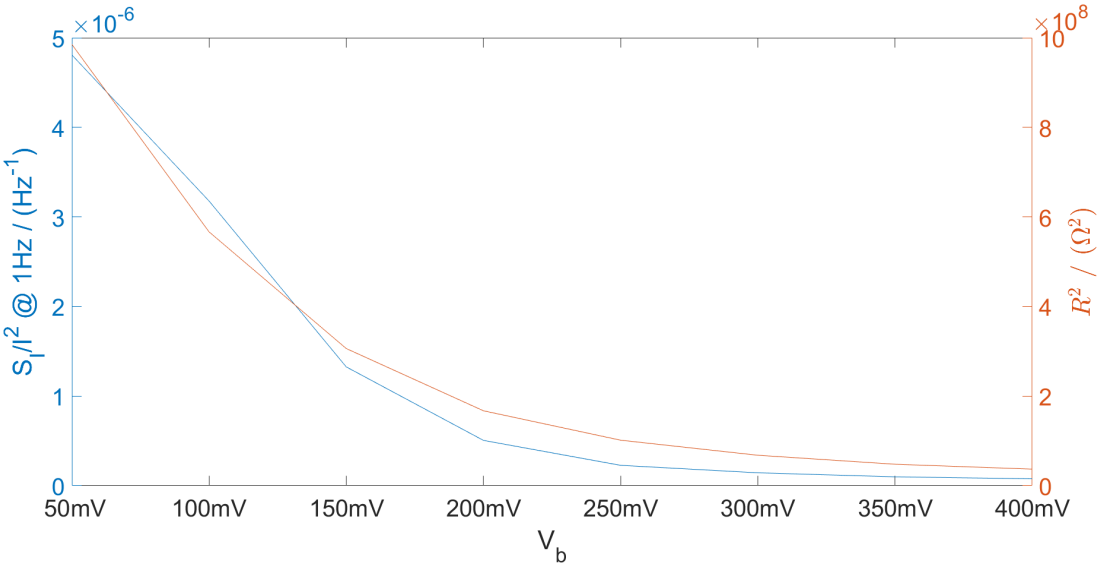

Figure 6.10: ***Comparison of the noise magnitude at*** $1\,\mathrm{Hz}$ ***and the resistance of a dGST300 PCM device for the SET state.***

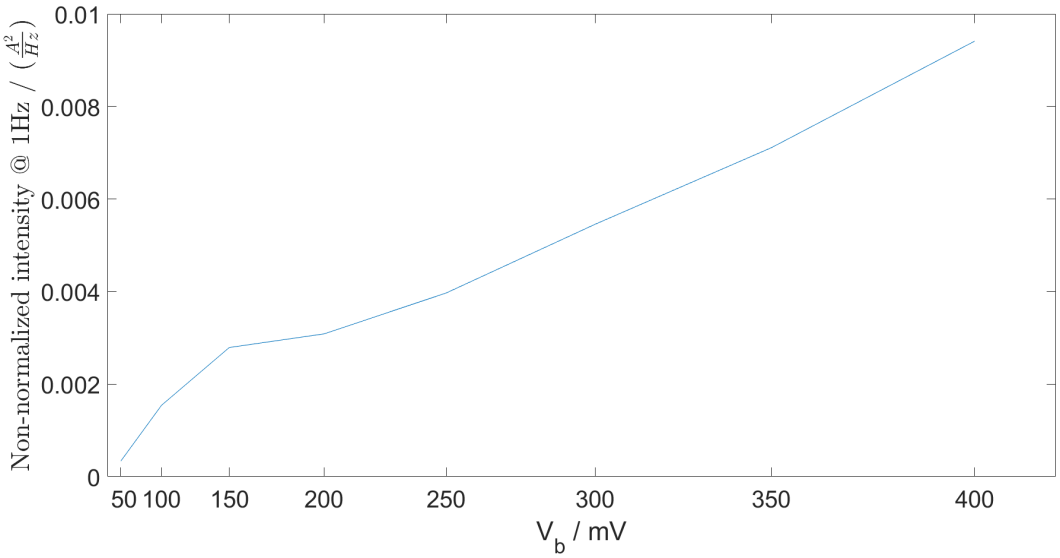

Figure 6.11: ***Non-normalized noise*** S_I ***vs squared applied bias voltage*** U^2 ***of a dGST300 PCM device for the SET state.***

6.5 Noise dependence on device cycling

Device cycling and endurance plays a critical role when building systems based on PCM devices. Not only is it important to ensure that the data stored on a device can be reliably obtained after an extended period of time, but it is even more important that the functionality of the device stays the same. The materials used for PCMs are composites of different elements that can potentially segregate over time which damages the device and could change the functionality over time. In addition, PCM devices undergo phase changes which cause mechanical stress that also contribute to device degradation. Because a PCM chip will operate with fresh devices as well as with devices that have undergone many phase transitions, it is very important to investigate the impact of the device degradation on the low-frequency noise. To this end we conducted an experiment where the 1/f noise was investigated for various states of cell cycling. RESET pulses are mostly responsible for the device degradation and therefore, the device cycling was simulated by applying many RESET pulses to the device, for example 1000. Figure 6.12 shows the observed noise during the cycling process for the RESET and the SET state. In Figure 6.12 one can see that the observed noise is changing throughout the cycling process. Firstly, the absolute magnitude is changing which might be due to a local change of the material composition [101] and secondly, there is a small dip forming at higher frequencies.

The changing noise magnitude might also be due to the changing resistance of the RESET and SET state. To investigate this in more detail, Figure 6.13 depicts a comparison of the noise magnitude at 1 Hz and the change in resistance. Also in this experiment, one can see a similar trends of the resistance and the change of the noise magnitude for the RESET and SET state.

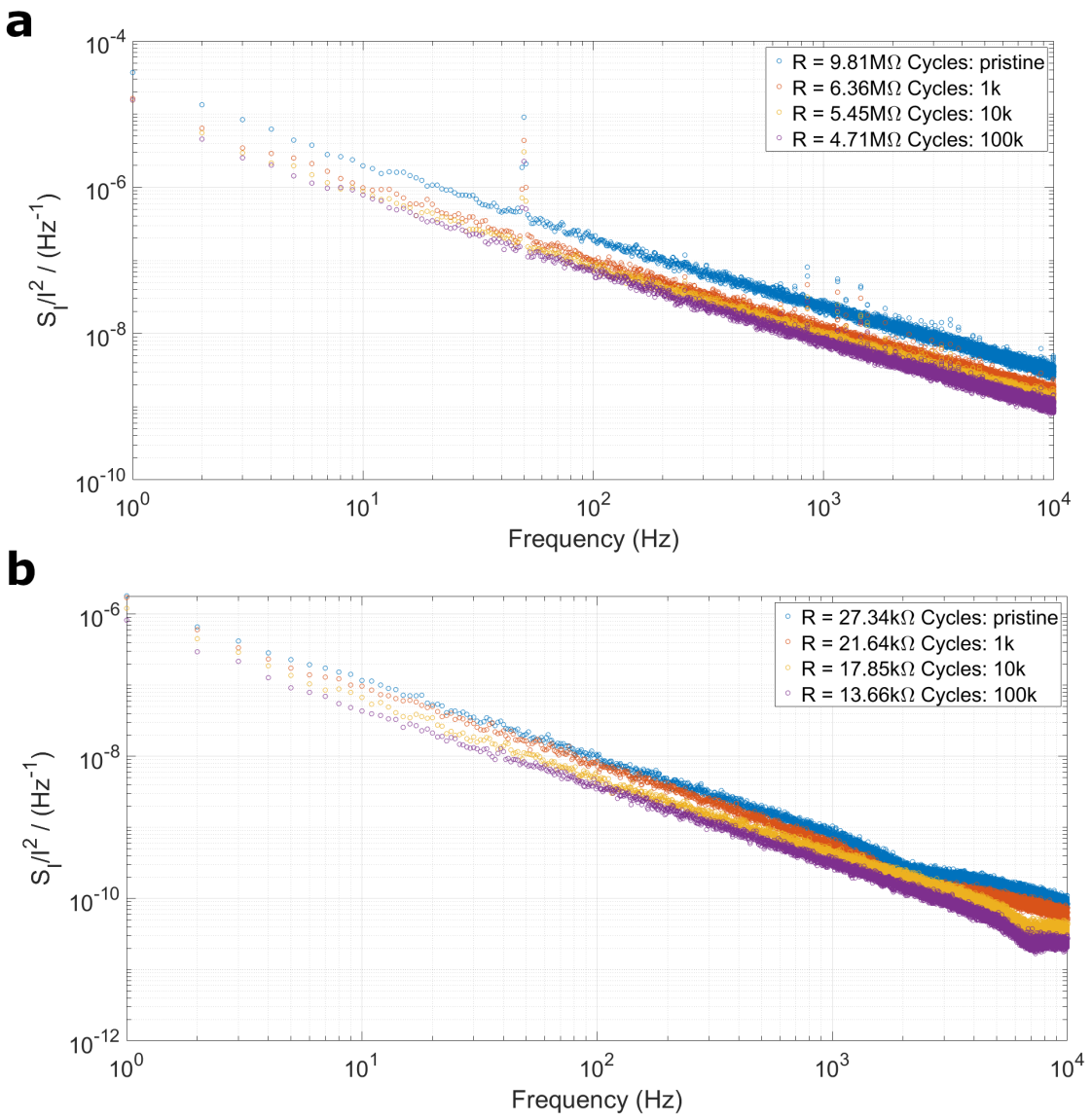

Figure 6.12: ***Noise spectra of a dGST300 PCM device under various cycling conditions.*** ***a*** *Normalized noise spectra for the RESET state.* ***b*** *Normalized noise spectra for the SET state.*

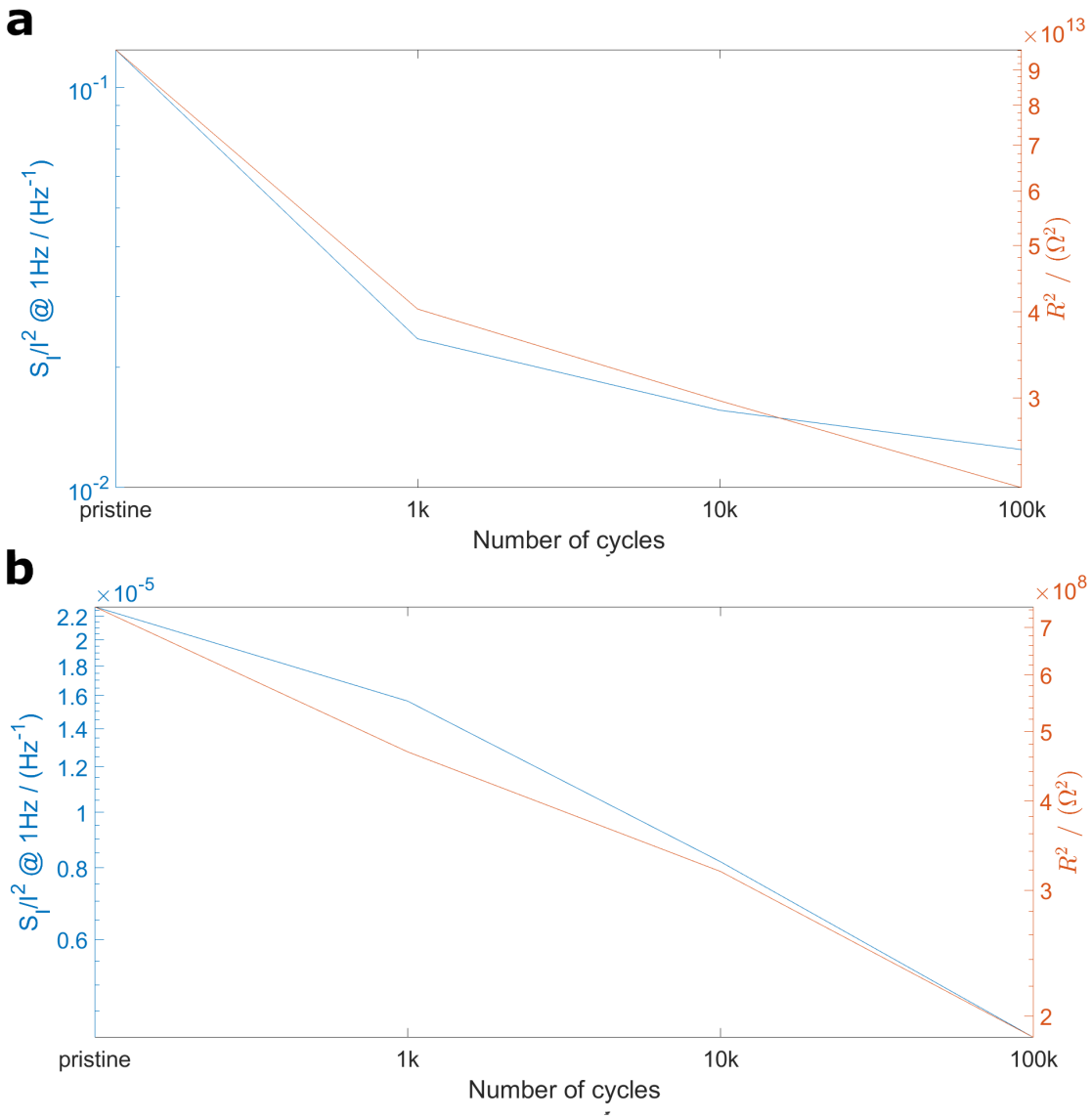

Figure 6.13: ***Comparison of the noise magnitude at*** $1\,\mathrm{Hz}$ ***and the resistance of a dGST300 PCM device.*** ***a*** *Comparison for the RESET state.* ***b*** *Comparison for the SET state.*

6.6 Noise dependence on temperature

The DWP model is able to make predictions for the behavior of the 1/f noise if the temperature T of the device is varied. This parameter can be used to gain more insights into the behavior of the PCM devices as it allows to predict the noise behavior in regimes where no noise measurements exists so far.

As the first step, the behavior of the resistance of the PCM as a function of temperature was investigated. This can give insights into the type material and the electronic transport behavior. As discussed in Section 2.2.6, the resistivity of the material determines whether the resistance will increase or decrease as a function of temperature. Figure 6.14 shows the resistance as a function of temperature of the PCM in the RESET state along with an Arrhenius fit $R(T) = R_0 \exp\left(\frac{E_a}{k_b T}\right)$, where the constant $R_0 = 3.2454 \cdot 10^4\,\Omega$ and the activation energy $E_a = 2.3163 \cdot 10^{-20}\,\mathrm{J} \sim 144.57\,\mathrm{meV}$. The resistance value at 300 K is 9.1 MΩ. To calculate the

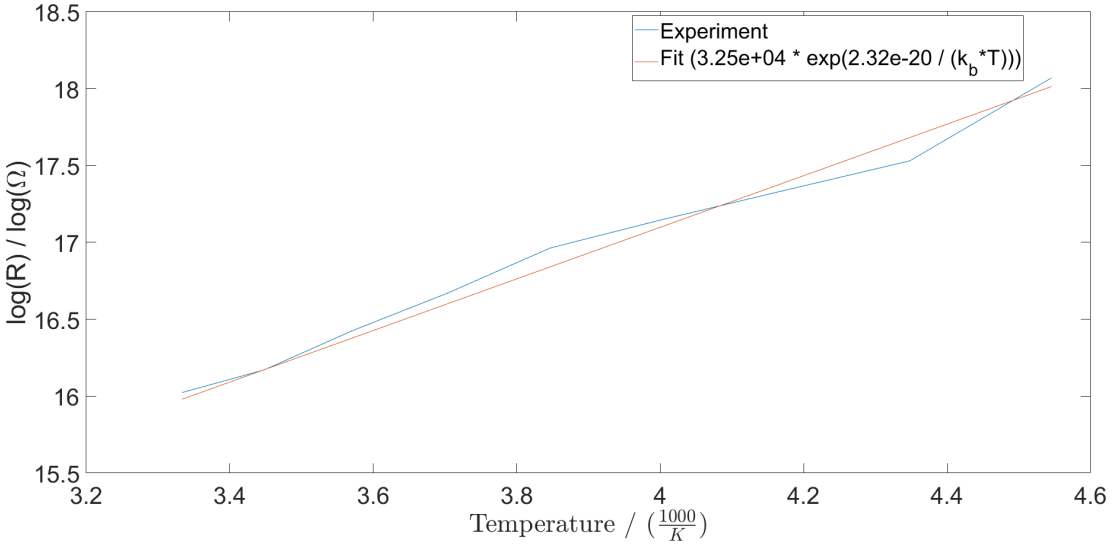

Figure 6.14: ***Resistance of the PCM as a function of temperature.*** *The behavior of the resistance was fit with an exponential function* $R(T) = 3.2454 \cdot 10^4 \exp\left(\frac{2.3163 \cdot 10^{-20}}{k_b T}\right)$ *(red dashed line).*

resistivity of the device, the geometry of the amorphous region is important. We assume that the amorphous region forms a hemispherical dome for which the resistance can be calculated as follows

$$R = \frac{\rho}{8 \cdot r_{BE}} + \frac{\rho}{2\pi}\left(\frac{1}{r_{BE}} - \frac{1}{r_{dome}}\right), \tag{6.1}$$

where ρ is the resistivity of the PCM device, r_{BE} is the radius of the bottom electrode and r_{dome} is the radius of the amorphous dome. Assuming typical values for the PCM device at hand, the resistivity is $\rho = 0.2317\,\Omega\mathrm{m}$, which is much higher than the threshold described in Section 2.2.6. Therefore, the resistance of the material is expected to increase.

As the next step, the noise behavior of the PCM is investigated under various temperatures. Since this experiment required temperatures below room temperature, it was carried out in the cryostat as described in Section 5.3. Figure 6.15 illustrates the PSD of the RESET state as a function of temperature. The PSD of the PCM decreases when the temperature increases, shown in Figure 6.15a. One potential reason for this is again the change of resistance with temperature. If one investigates the PSD at low frequencies in this setting, one can also observe a trend that follows the squared resistance of the device, shown in Figure 6.15b. However, it

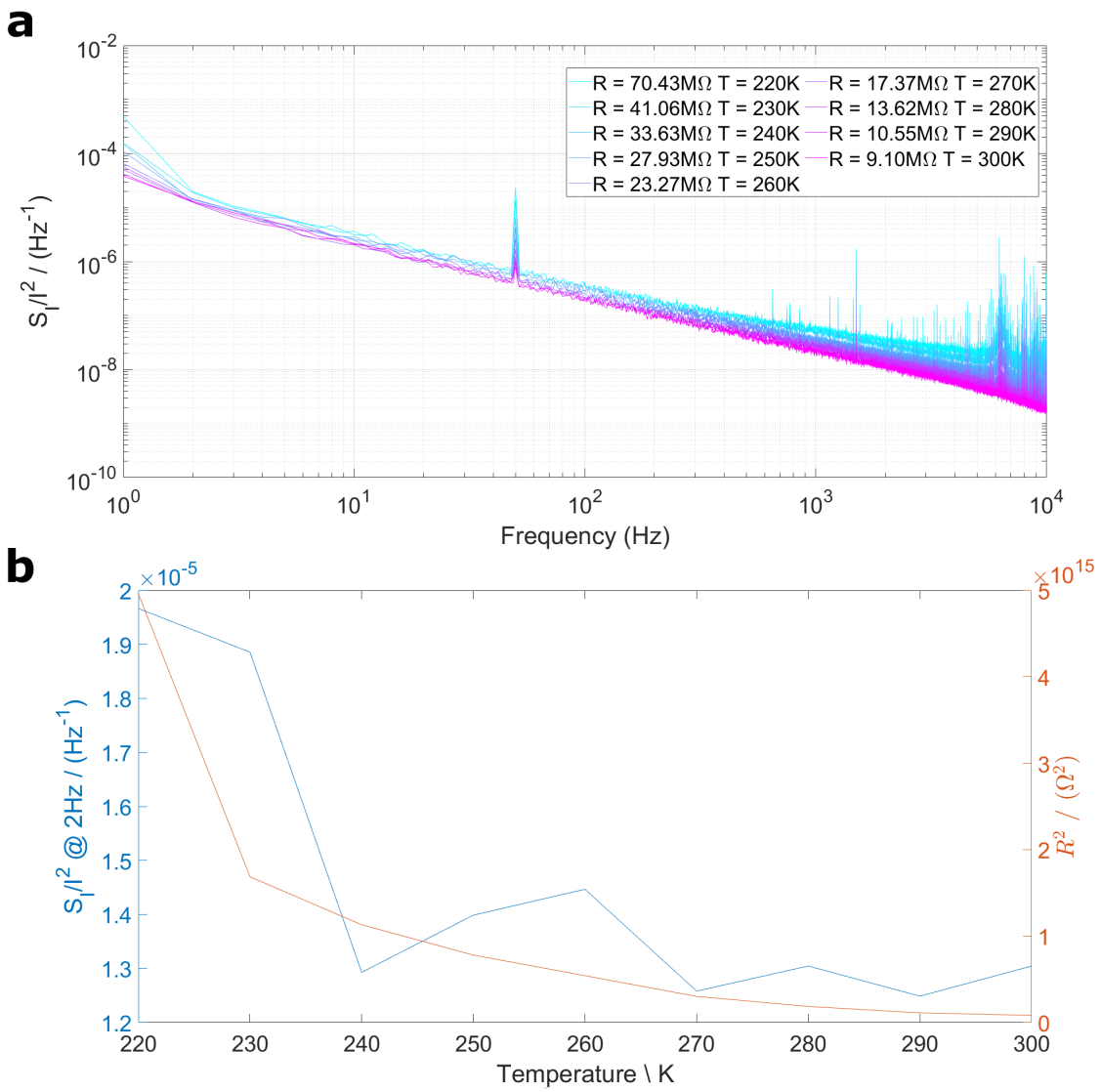

Figure 6.15: ***Analysis of the temperature dependence of the PSD of the RESET state.*** ***a*** *PSD of the RESET state various temperatures.* ***b*** *PSD at* 1 Hz *for various temperatures along with the squared resistance of the device.*

was observed that the noise rapidly increased at 1Hz which is potentially due to an artifact in the measurement setup. Therefore, the investigations were done at 2 Hz, where the noise was measured more reliably. The trend is very similar to the one that is observed in Figure 6.10, where the bias voltage of the cell is varied.

Afterwards the observed noise is compared to the theoretical model. Figure 6.16 shows the predicted noise spectra for selected temperatures. One can see that the model predicts an opposite temperature dependence than the one that is observed experimentally, see Figure 6.15. If the temperature decreases, the model predicts that the noise also decreases rather than increases. This is because the model might be too simple. The temperature influences the prefactor and

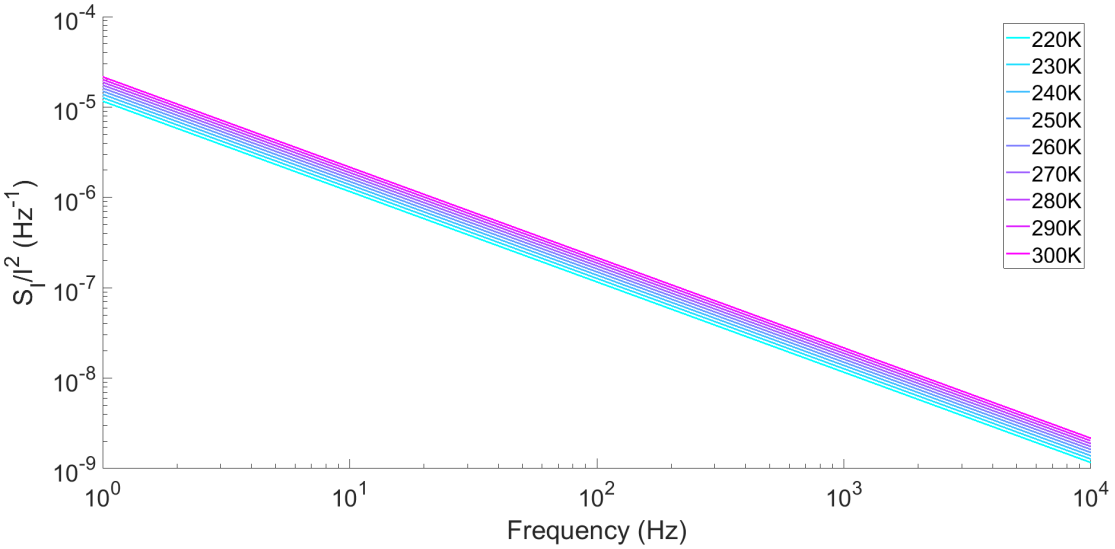

Figure 6.16: ***Simulated PSDs for various temperatures.***

the multiplicative exponent in

$$S(f) = \frac{N_0 k_b^2 T^2}{f \cdot (W_{B,max} - W_{B,min})} \cdot \tag{6.2}$$

$$\left[arctan\left(\tau_0 \cdot f \cdot exp\left(\frac{W_{B,max}}{k_b T}\right)\right) - arctan\left(\tau_0 \cdot f \cdot exp\left(\frac{W_{B,min}}{k_b T}\right)\right)\right] \tag{6.3}$$

see Chapter 4 Equation 4.14, but for example does not influence the prefactor N_0. As shown in Figure 6.14, a change of temperature also causes the resistance of the PCM device to change which is not directly reflected in the model.

7
Discussion and Outlook

A major part of this work was to build up two separate platforms that can be used to conduct noise measurements. One can operate at room temperature and elevated temperatures, while the second one mainly operates at cryogenic temperatures. Using these setups, different noise measurements have been conducted that investigated various applied bias voltages, different materials, different aging states of the device as well as cryogenic temperatures. The observed data was compared to the predictions of the simple theoretical model. Although the DWP model could fit the observed noise spectra as well as the slope reasonably well, it predicted the wrong temperature behavior. It also predicted pronounced frequency roll-offs at high and low frequencies, which were not as present in the conducted experiments. Overall, there are too many factors that are not properly captured by this simplistic model, for example the bias voltage dependence of the resistance or self-heating effects are not captured properly. Therefore, the employed model might just be too simple to capture the real physical phenomena underlying the 1/f noise. Very interestingly, however, one can observe a common trend across all measurements, which suggests that the magnitude of the low-frequency noise scales with the squared resistance of the device.

Two effects that affect the resistance of the device were investigated more closely, namely different bias voltages and different temperatures. In both experiments the same trend of the noise magnitude was observed. Ideally, these effects must be separated to study them individually and because they could potentially influence each other. The bias voltage dependent analysis may not have provided enough separation, as the bias affected the resistance, as well as the temperature increase due to self-heating of the device. However, the temperature dependent experiment in the cryostat provided some separation of these two effects, as only the temperature was changed.

To further verify these findings in the future, more conclusive experiments can be carried out. In one promising experiment the temperature influence and the bias voltage influence on the resistance value of the PCM device cancel out. This could be achieved by setting the PCM device into a particular state and then measuring the low-frequency noise at different temperatures and applied bias voltages, while keeping the resistance of the device at the same value. For example, if the temperature is decreased and the resistance of the device would increase, one could apply a higher bias voltage, so that the resistance level stays the same. This experiment would target the hypothesis that the noise magnitude scales with the resistance value.

A similar idea can be pursued in a different experiment. In this experiment, line PCM devices are measured. The resistance of such devices can be tuned by the geometry. One can then apply different bias voltages or different temperatures and prepare the line devices in such a way that always the same resistance results. This would involve a lot of effort, since for every bias voltage or temperature a separate device has to be fabricated. On the other hand, this experiment would allow to study the influence of the bias voltage and the temperature separately.

In addition, working on the line PCM device would allow to also study the question whether the noise is a bulk or a surface effect. With this type of cell, it would be possible to change the ratio between volume and surface by changing the aspect ratio. Therefore, surface effects could be made stronger or less pronounced in an experiment.

Another open question is whether the noise is a state-dependent effect. The state of the PCM

cell can in principle be created in two ways. Either the state is created by gradually crystallizing an amorphous PCM device or the other way around, by creating amorphous regions within the polycrystalline PCM. Although similar resistance values could be achieved in both procedures, the observed noise may be different, because the phase configurations are different.

Bibliography

[1] R. F. Freitas and W. W. Wilcke, IBM J. Res. Dev. **52**, 439 (2008).

[2] G. Fettweis and E. Zimmermann, Proceedings of the 11th international symposium on wireless personal multimedia communications , 6 (2008).

[3] K. Kambatla, G. Kollias, V. Kumar, and A. Grama, J. Parallel Distrib. Comput. **74**, 2561 (2014).

[4] M. D. Assunção, R. N. Calheiros, S. Bianchi, M. A. S. Netto, and R. Buyya, J. Parallel Distrib. Comput. **79-80**, 3 (2015).

[5] J. C. Augusto, SpringerLink , 213 (2007).

[6] J. S. Meena, S. M. Sze, U. Chand, and T.-Y. Tseng, Nanoscale Res. Lett. **9**, 526 (2014).

[7] M. Wuttig and N. Yamada, Nat. Mater. **6**, 824 (2007).

[8] A. Athmanathan, M. Stanisavljevic, N. Papandreou, H. Pozidis, and E. Eleftheriou, IEEE J. Emerging Sel. Top. Circuits Syst. **6**, 87 (2016).

[9] A. Lotnyk, M. Behrens, and B. Rauschenbach, Nanoscale Adv. **1**, 3836 (2019).

[10] L. Chua, IEEE Transactions on Circuit Theory **18**, 507 (1971).

[11] S. S. P. Parkin et al., Nat. Mater. **3**, 862 (2004).

[12] S. Yuasa, T. Nagahama, A. Fukushima, Y. Suzuki, and K. Ando, Nat. Mater. **3**, 868 (2004).

[13] D. Apalkov, B. Dieny, and J. M. Slaughter, Proc. IEEE **104**, 1796 (2016).

[14] S. Hamdioui et al., 2019 Design, Automation & Test in Europe Conference & Exhibition (DATE) , 486 (2019).

[15] A. J. Smith, ACM Comput. Surv. **14**, 473–530 (1982).

[16] D. Ielmini and H.-S. P. Wong, Nat. Electron. **1**, 333 (2018).

[17] A. Sebastian, M. L. Gallo, and E. Eleftheriou, J. Phys. D: Appl. Phys. **52**, 443002 (2019).

[18] J. J. Yang, D. B. Strukov, and D. R. Stewart, Nat. Nanotechnol. **8**, 13 (2012).

[19] W. B. Davenport, Jr., W. L. Root, and G. Weiss, *An Introduction to the Theory of Random Signals and Noise*, volume 11, American Institute of Physics, 1958.

[20] H. Nyquist, Phys. Rev. **32**, 110 (1928).

[21] J. B. Johnson, Phys. Rev. **32**, 97 (1928).

[22] W. Schottky, Ann. Phys. **362**, 541 (1918).

[23] F. N. Hooge and A. M. H. Hoppenbrouwers, Physica **42**, 331 (1969).

[24] F. N. Hooge and A. M. H. Hoppenbrouwers, Physica **45**, 386 (1969).

[25] M. von Haartman and M. Östling, SpringerLink , 27 (2007).

[26] P. Stoica and R. L. Moses, *Spectral analysis of signals*, Upper Saddle River, N.J. : Pearson/Prentice Hall, 2005., 2005.

[27] N. Wiener, Acta Mathematica **55**, 117 (1930).

[28] A. Khintchine, Math. Ann. **109**, 604 (1934).

[29] J. B. Johnson, Phys. Rev. **26**, 71 (1925).

[30] M. A. Caloyannides, J. Appl. Phys. **45**, 307 (1974).

[31] T. Musha and M. Yamamoto, *1/f fluctuations in biological systems*, volume 6, 1997.

[32] R. T. Baillie, Journal of Econometrics **73**, 5 (1996).

[33] M. J. Uren, D. J. Day, and M. J. Kirton, Appl. Phys. Lett. **47**, 1195 (1985).

[34] Z. Li et al., Sci. Rep. **8**, 1 (2018).

[35] D. Fugazza, D. Ielmini, S. Lavizzari, and A. L. Lacaita, 2010 IEEE International Reliability Physics Symposium , 743 (2010).

[36] A. V. Kolobov, J. Tominaga, and P. Fons, *Phase-Change Memory Materials*, pages 1–1, Springer International Publishing, Cham, 2017.

[37] S. R. Ovshinsky, Phys. Rev. Lett. **21**, 1450 (1968).

[38] S. Hudgens and B. Johnson, MRS Bulletin **29**, 829–832 (2004).

[39] J. Hellmig, A. Mijiritskii, H. J. Borg, P. Vromans, and K. Musialkova, *Dual-layer Blu-ray Disc based on fast-growth phase-change materials*, IEEE, 2002.

[40] P. Rausch, *Investigations of binary and ternary phase change alloys for future memory applications*, PhD thesis, Aachen, 2012, Prüfungsjahr: 2012. - Publikationsjahr: 2013; Aachen, Techn. Hochsch., Diss., 2012.

[41] V. E. Madhavan, M. Carignano, A. Kachmar, and K. S. Sangunni, Sci. Rep. **9**, 1 (2019).

[42] P. Guo, A. M. Sarangan, and I. Agha, Appl. Sci. **9**, 530 (2019).

[43] Y. Lai et al., J. Electron. Mater. **34**, 176 (2005).

[44] S. W. Ryu et al., Appl. Phys. Lett. **92**, 142110 (2008).

[45] P. Guo et al., Appl. Phys. Lett. **116**, 131901 (2020).

[46] Q. Wang et al., J. Phys. Chem. C **123**, 30640 (2019).

[47] S. Kikuchi et al., *Preparation of Oxygen-doped and Nitrogen-doped Ge-Sb-Te System Thin Film for Phase Change Random Access Memory by RF Magnetron Sputtering*, IEEE, 2006.

[48] W. J. Wang et al., Appl. Phys. Lett. **93**, 043121 (2008).

[49] D. Krebs et al., J. Appl. Phys. **106**, 054308 (2009).

[50] A. Redaelli, A. Pirovano, A. Benvenuti, and A. L. Lacaita, J. Appl. Phys. **103**, 111101 (2008).

[51] A. Sebastian, N. Papandreou, A. Pantazi, H. Pozidis, and E. Eleftheriou, J. Appl. Phys. **110**, 084505 (2011).

[52] N. Yamada and T. Matsunaga, J. Appl. Phys. **88**, 7020 (2000).

[53] S. Privitera, C. Garozzo, A. Alberti, L. Perniola, and B. De Salvo, AIP Adv. **3**, 012105 (2013).

[54] S. K. O'Leary, S. R. Johnson, and P. K. Lim, J. Appl. Phys. **82**, 3334 (1997).

[55] P. A. Lee and T. V. Ramakrishnan, Rev. Mod. Phys. **57**, 287 (1985).

[56] C. Longeaud et al., J. Appl. Phys. **112**, 113714 (2012).

[57] G. W. Burr et al., Journal of Vacuum Science & Technology B, Nanotechnology and Microelectronics: Materials, Processing, Measurement, and Phenomena **28**, 223 (2010).

[58] M. Le Gallo, M. Kaes, A. Sebastian, and D. Krebs, New J. Phys. **17**, 093035 (2015).

[59] M. Le Gallo, *Phase-Change Memory: Device Physics and Application to non-von Neumann Computing*, PhD thesis, ETH Zurich, 2017.

[60] R. G. D. Jeyasingh, D. Kuzum, and H.-S. P. Wong, 2011 3rd IEEE International Memory Workshop (IMW) (2011).

[61] A. B. Kaiser, Rep. Prog. Phys. **64**, 1 (2001).

[62] J. H. Mooij, Phys. Status Solidi A **17**, 521 (1973).

[63] C. C. Tsuei, Phys. Rev. Lett. **57**, 1943 (1986).

[64] A. M. Jayannavar and N. Kumar, Phys. Rev. B **37**, 573 (1988).

[65] M. Le Gallo and A. Sebastian, J. Phys. D: Appl. Phys. **53**, 213002 (2020).

[66] M. L. Gallo, D. Krebs, F. Zipoli, M. Salinga, and A. Sebastian, Adv. Electron. Mater. **4**, 1700627 (2018).

[67] G. W. Burr et al., IEEE J. Emerging Sel. Top. Circuits Syst. **6**, 146 (2016).

[68] W. W. Koelmans et al., Nat. Commun. **6**, 1 (2015).

[69] F. Zipoli and A. Curioni, New J. Phys. **15**, 123006 (2013).

[70] J. Y. Raty et al., Nat. Commun. **6**, 1 (2015).

[71] S. Gabardi, S. Caravati, G. C. Sosso, J. Behler, and M. Bernasconi, Phys. Rev. B **92**, 054201 (2015).

[72] H. Pozidis et al., 2012 4th IEEE International Memory Workshop , 1 (2012).

[73] P. Fantini, A. Pirovano, D. Ventrice, and A. Redaelli, Appl. Phys. Lett. **88**, 263506 (2006).

[74] M. Nardone, V. I. Kozub, I. V. Karpov, and V. G. Karpov, Phys. Rev. B **79**, 165206 (2009).

[75] P. Fantini et al., 2008 IEEE International Electron Devices Meeting , 1 (2008).

[76] G. F. Close et al., 2010 International Electron Devices Meeting , 29.5.1 (2010).

[77] G. B. Beneventi, *Characterization and modeling of phase-change memories*, PhD thesis, Université de Grenoble, 2011.

[78] S. Kim et al., IEEE Trans. Electron Devices **63**, 3922 (2020).

[79] G. Betti Beneventi, A. Calderoni, P. Fantini, L. Larcher, and P. Pavan, J. Appl. Phys. **106**, 054506 (2009).

[80] R. F. Voss and J. Clarke, Phys. Rev. B **13**, 556 (1976).

[81] A. L. a. L. Mcwhorter, *1/f noise and related surface effects in germanium*, PhD thesis, Massachusetts Institute of Technology, 1955.

[82] F. N. Hooge, Phys. Lett. A **29**, 139 (1969).

[83] A. Mircea, A. Roussel, and A. Mitonneau, Phys. Lett. A **41**, 345 (1972).

[84] F. N. Hooge, Physica **60**, 130 (1972).

[85] Th. G. M. Kleinpenning, Physica **77**, 78 (1974).

[86] L. K. J. Vandamme, Phys. Lett. A **49**, 233 (1974).

[87] P. Dutta and P. M. Horn, Rev. Mod. Phys. **53**, 497 (1981).

[88] J. Bernamont, Proc. Phys. Soc. **49**, 138 (1937).

[89] P. Bak, C. Tang, and K. Wiesenfeld, Phys. Rev. Lett. **59**, 381 (1987).

[90] M. B. Weissman, Rev. Mod. Phys. **60**, 537 (1988).

[91] F. N. Hooge, IEEE Transactions on Electron Devices **41**, 1926 (1994).

[92] I. V. Karpov et al., J. Appl. Phys. **102**, 124503 (2007).

[93] S. Machlup, J. Appl. Phys. **25**, 341 (1954).

[94] Yu. M. Galperin, V. G. Karpov, and V. I. Kozub, Adv. Phys. **38**, 669 (1989).

[95] P. w. Anderson, B. I. Halperin, and C. M. Varma, Philosophical Magazine: A Journal of Theoretical Experimental and Applied Physics **25**, 1 (1972).

[96] P. W. Anderson, Phys. Rev. Lett. **34**, 953 (1975).

[97] M. Nardone, Theories of Charge Transport and Nucleation in Disordered Systems, 2011, [Online; accessed 3. Apr. 2020].

[98] G. Betti Beneventi, M. Ferro, and P. Fantini, IEEE Electron Device Letters **33**, 1559 (2012).

[99] M. Boon, Technical Report (2016).

[100] P. Welch, IEEE Trans. Audio Electroacoust. **15**, 70 (1967).

[101] W. Kim et al., 2016 IEEE International Electron Devices Meeting (IEDM) , 4.2.1 (2016).